NIST Technical Note
NIST TN 2249

A Gray-Box Model of a Two-Stage Heat Pump for Electrical Load Forecasting in a Single-Family Residence

Farhad Omar, Ph.D.

NIST NATIONAL INSTITUTE OF
STANDARDS AND TECHNOLOGY
U.S. DEPARTMENT OF COMMERCE

A Gray-Box Model of a Two-Stage Heat Pump for Electrical Load Forecasting in a Single-Family Residence

Farhad Omar, Ph.D.
Building Energy and Environment Division
Engineering Laboratory

NIST TN 2249
March 2023

Certain commercial entities, equipment, or materials may be identified in this document in order to describe an experimental procedure or concept adequately. Such identification is not intended to imply recommendation or endorsement by the National Institute of Standards and Technology, nor is it intended to imply that the entities, materials, or equipment are necessarily the best available for the purpose.

NIST Technical Series Policies
[Copyright, Fair Use, and Licensing Statements](#)
[NIST Technical Series Publication Identifier Syntax](#)

Publication History
Approved by the NIST Editorial Review Board on 2023-03-09

NIST Author ORCID iDs
Farhad Omar: 0000-0002-0618-0060

Contact Information
farhad.omar@nist.gov

Abstract

Buildings as a set of electric loads and generation resources can play an essential role in managing the stability of the power system in a smart grid. Traditionally, buildings assumed a passive role in the day-to-day operation of the electric grid, with utilities controlling the supply of energy to match the demand for buildings. However, the dynamics of the power distribution grid are rapidly changing. A critical aspect of managing the balance between supply and demand in the distribution grid is estimating future demand through load forecasting. Load forecasting requires accurate, adaptive, and simple models to account for the dynamic behavior of the electrical demand. In residential buildings, heat pumps are a significant source of energy consumption. This document describes a novel gray-box model (RL Model) to forecast the steady-state and transient current consumption for a two-stage, air-source heat pump in heating and cooling seasons. The RL Model is derived from a solution of a first-order differential equation describing the voltage and outdoor temperature dependent characteristics of a resistor-inductor equivalent circuit. Key parameters of the RL Model were estimated using a learning algorithm. The performance of the RL Model is validated using measurement data from the Net-Zero Energy Residential Test Facility located on the National Institute of Standards and Technology (NIST) campus in Gaithersburg, MD. The predicted output of the RL Model, current consumption, is used to estimate the heat pump's real and reactive power consumption for different operating stages and seasons. A list of key parameters, e.g., the time constant and temperature-dependent coefficients of the RL Model, are tabulated. Knowledge of the time constant provides critical information for analyzing the aggregated effect of controlling many heat pumps as flexible loads on grid stability and provision of ancillary services. The average root mean squared error between the RL Model's predicted current output and the measured current consumption is 0.06.

Keywords

Table of Contents

List of Tables

List of Figures

1. Introduction

The electrical grid is undergoing significant changes due to a two-way flow of energy and information. Buildings as a set of electric loads and generation resources can be essential in managing grid stability and supporting decarbonization efforts while maintaining thermal comfort and reducing cost. Usually, buildings assumed a passive rule in the day-to-day operation of the electric grid, with utilities controlling the supply of energy to match the demand for buildings. However, the dynamic behavior of the power distribution grid is rapidly changing. These changes are due to the integration of renewable energy sources, the proliferation of electric vehicles, including electric storage, and the dynamic behavior of energy-consuming loads [1, 2].

Recent studies show that building loads can provide ancillary services such as voltage control, frequency regulation, reserve, and load following to maintain grid stability [2–5]. Grid stability also requires a balance between supply and demand for electricity. An essential component of managing grid stability is forecasting the expected load. Load forecasting enables utility planners, aggregators, and customers to devise mitigating control strategies for efficient and cost-effective grid operation. Developing effective and adaptive control strategies requires accurate load models for capturing the dynamic behavior of the electrical load. Load modeling is a critical component of power system studies [4, 6–8].

Traditionally, utilities relied on aggregated load models to maintain the grid's stability by managing the balance between supply and demand, encompassing the residential, commercial, and industrial sectors. However, the proliferation of energy-efficient and flexible non-linear loads [9], integration of renewable energy sources, and demand-side management implementation highlighted the need to update the existing load model [8]. In power system studies, electrical load modeling can broadly be classified into static and dynamic approaches [8, 9]. Static models describe the instantaneous real and reactive power consumptions as a function of the bus voltage magnitudes and system frequency. These models, such as power flow studies, are typically used for steady-state analysis. In contrast, dynamic load models are used for stability analysis because they exhibit a time-dependent response to changes in the voltage and frequency of the system. A comprehensive of review of load modeling approaches for power system studies are presented in [8, 9].

Heating, ventilating, and air-conditioning (HVAC) is one of the largest electrical loads in a typical building. Air-source heat pumps are a common type of HVAC equipment in residential homes and are typically the largest load. It is important to predict the electrical energy consumption of the air-source heat pumps to evaluate control strategies involving demand response, voltage control, frequency regulation, or reserve for grid stability or delivery of ancillary services. A review of heat pump modeling and control strategies used for ancillary services and grid stability is provided in [3, 10–12].

There are many ways to model the performance of residential heat pumps [13]. However, for modeling the performance of a heat pump, the three most common approaches are: physics-based (white-box), data-driven (black-box), and a hybrid of physics-based and data-driven (gray-box) models [8, 9, 13]. Developing a white-box model requires detailed knowledge of the underlying physical principles governing the operation of a heat pump and its components. In contrast, black-

box models are purely data-driven. Black-box models lack knowledge of the underlying physical structure of the components of a heat pump and their operation. These models require a large dataset for training and learning purposes and do not provide a precise meaning for the underlying physics of the units. Gray-box modeling is a hybrid method often developed based on a simplified version of the physical process using equivalent circuits and measurement data. Measurement data is used to estimate the parameters of the simplified physics-based model. The gray-box models do not require a large set of data for training. Another advantage of the gray-box approach is that it can provide a clear physical meaning for specific parameters of the model compared to the black-box model of the same process. Gray-box models are also more adaptable because the values of new parameters can be estimated from a different dataset, capturing the unique characteristics of another residential heat pump.

Essential components of a heat pump include an evaporator, a compressor, a condenser, an expansion valve, and power electronics. Generally, it is hard to model the exact characteristics of individual heat pump components and describe their overall impact on power consumption. Therefore, a common technique, in power system studies, for capturing the overall performance of a heat pump is to create a lumped model, representing the combined effect of individual components. These lumped techniques include using equivalent circuit representation of an induction motor (IM) [8, 9, 14, 15], exponential and polynomial ZIP (constant impedance, constant current, and constant power, respectively), and composite load models (ZIP + IM) [8, 9, 16] to model residential heat pumps. Poudel et al. [14] presented an aggregate model of single-phase induction motors to represent residential heat pump loads in steady-state and transient operation for fault analysis. The aggregated model was derived by combining equivalent circuit models of single-phase induction motors. The parameters of the aggregate equivalent circuit were determined from no-load and locked rotor tests. Schneider et al. [17] presented a multi-state (off, cooling, heating-normal, and heating-auxiliary) model of a residential heat pump. The multi-state model in [17] is a single-stage heat pump that provides thermal energy as a function of heat flow rate through the cooling unit and the compressor's electrical losses. The heat flow rate is obtained from the heat transfer equations describing the mechanical torque of the compressor. The electrical losses of the compressor are captured by an equivalent circuit model of a split-phase IM.

However, using the IM and ZIP+IM models to represent many heat pumps for power system studies and simulation is computationally expensive because they contain many parameters. ZIP models can only describe the on or off state of a heat pump's operation [17] and capture the steady-state power consumption. ZIP models are inadequate to properly capture the dynamic behavior of heat pumps. ZIP models are insufficient because a heat pump's energy consumption is not only a function of terminal voltage but also a function of the outdoor temperature and control algorithms used to manage the heating and cooling operation. Therefore, a simpler approach is needed to model the operation of a heat pump that might be used in a residential home.

In this work, a novel gray-box model for predicting the current consumption of a two-stage heat pump in a single-family residence was developed. The approach was to define a simple resistor-inductor (RL Model) equivalent circuit and modify it to account for the outdoor temperature's impact on the heat pump's power consumption in both transient and steady-state conditions. A learning algorithm (LA) was defined to learn the key parameters of the RL Model using measurement data instead deriving them from detailed knowledge of the physical thermal and electrical characteristics of the heat pump. The performance of the RL Model was validated using

performance measurements from the Net-Zero Energy Residential Test Facility (NZERTF) at the National Institute of Standards and Technology (NIST) in Gaithersburg, Maryland [18, 19]. The NZERTF house is a typical four-bedroom house in the Washington DC metro area with a detached garage. The exterior of the NZERTF is shown in Fig. 1.

Fig. 1. The NZERTF exterior

The main objectives of this technical note are:

1. To provide a brief description of the data acquisition setup for measuring the performance of a two-stage air-source heat pump in the NZERTF,
2. To describe a first-order RL Model for estimating the steady-state and transient current consumption of the heat pump in both heating and cooling seasons,
3. To describe the LA used for estimating the coefficients of the first-order RL Model, and
4. To estimate the heat pump's real and reactive power consumption using its predicted current consumption, measured line voltage, and displacement power factor.

2. Measuring the Electrical Performance of a Two-Stage Air-Source Heat Pump

The main objectives of this research were realized by simultaneously measuring the performance of the air-source heat pump at the main circuit breaker panel inside the NZERTF and on the utility side of the meter located outside of the NZERTF. Fig. 2 shows a schematic representation of the monitoring approach. It shows a typical split-phase configuration of alternating current (AC) 240 V nominal voltage of power distribution in residential homes in the U.S. In this configuration, power is supplied to various loads inside the NZERTF by two live (hot) wires, designated Line 1 (L1) and Line 2 (L2). A neutral (N) wire carries the current difference between L1 and L2. In an ideal and balanced system, zero current flows through the neutral wire. The split-phase configuration supports 240 V (line-to-line) and 120 V (line-to-neutral) loads. Typically, the L1, L2, and N cables are color-coded as black, red, and white, respectively. Installation of the ground

connection (green cable not shown in the schematic) is a national electric code requirement in buildings.
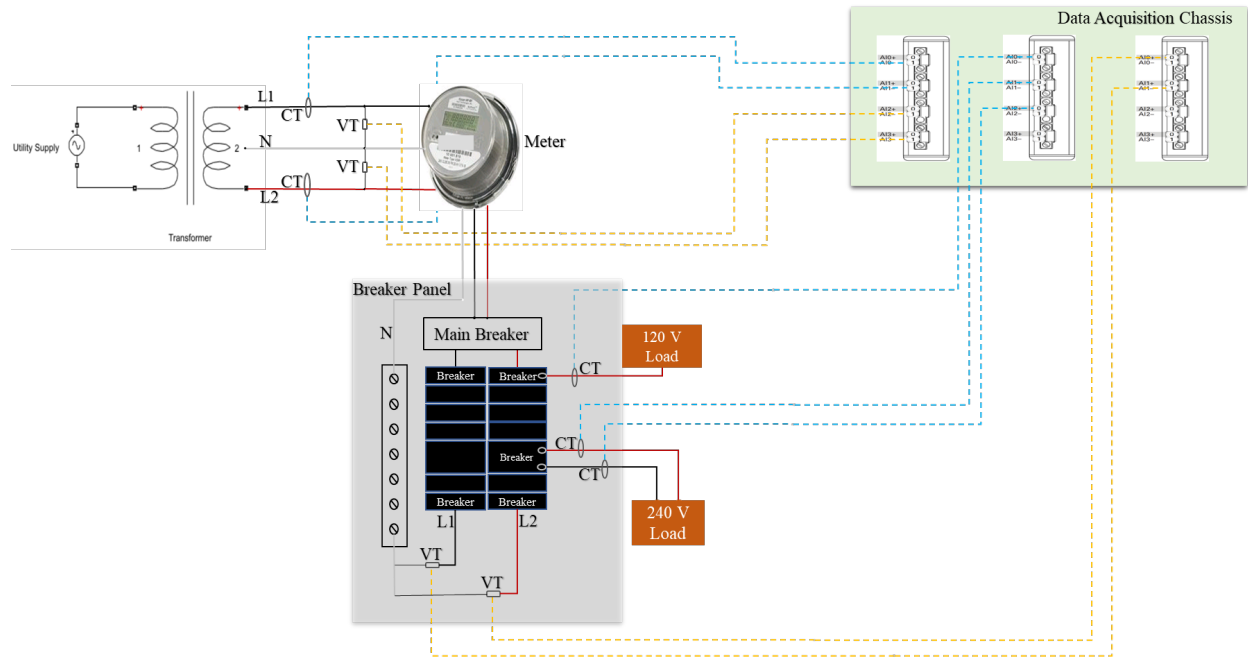
Fig. 2. Schematic representation of the sensors placement for measuring the voltage and current waveforms of various appliances in the NZERTF

A detailed description of the experimental design for measuring the voltage and current waveforms of various appliances, the uncertainty of measurement, and the gain and frequency response of the sensors are documented in [20]. A list of relevant sensor types, maximum ratings, functionalities, and abbreviated designations are shown in Table 1. In this study, the root mean square (RMS) outputs of the sensors on the utility side of the meter, as shown in Fig. 2, were used to model the performance of the air-source heat pump.

Table 1. Sensor Designations

Sensor Designation	Measurement Function	Type Description
CT_1	Current	Magnetic Induction (300 A RMS)
CT_2	Current	Magnetic Induction (120 A RMS)
VT_1	Voltage	Passive voltage divider (300 V RMS)
VT_2	Voltage	Passive voltage divider (300 V, peak)

As shown in Table 1, there are two voltage transducers (VTs) and two clamp-on current transducers (CTs). The outputs of the sensors are scaled analog voltages of the inputs. Current sensors CT_1 and CT_2 are magnetic induction transducers. These sensors do not require external power supplies to operate. Similarly, voltage sensors VT_1 and VT_2 are single-ended passive voltage dividers that do not require external power supplies. These voltage dividers measure the potential difference between a line and the ground or neutral (N) in buildings. In residential homes,

the ground and neutral wires are directly tied inside the main circuit breaker panel; therefore, all voltage measurements were conducted between lines L1 and L2 and the neutral.

2.1.   Current and Voltage Waveform of the Air-Source Heat Pump

The air-source heat pump requires a 240 V AC power supply. It has two main components, an air-handling unit inside the house and an outdoor unit containing a compressor and a coil that serves as an evaporator in the heating mode and as a condenser in the cooling mode. The air-handling unit uses a variable-speed blower to provide conditioned air to all areas of the home. The outdoor unit utilizes a two-stage scroll compressor to provide different heating or cooling capacities. The waveform current consumption of the air-source heat pump for the heating season is shown in Fig. 3. Fig. **3** shows two cycles of the voltage and current waveforms recorded between L1-N and L2-N during the 1st Stage, 2nd Stage, and 3rd Stage of the heat pump operation in the heating mode. In the cooling season, the heat pump's electrical performance data show similar waveform patterns as shown in Fig. 3. However, in the cooling season, the heat pump only operates in the 1st Stage or 2nd Stage, and there is no auxiliary or 3rd Stage. For brevity, the plots for the cooling season are not shown.
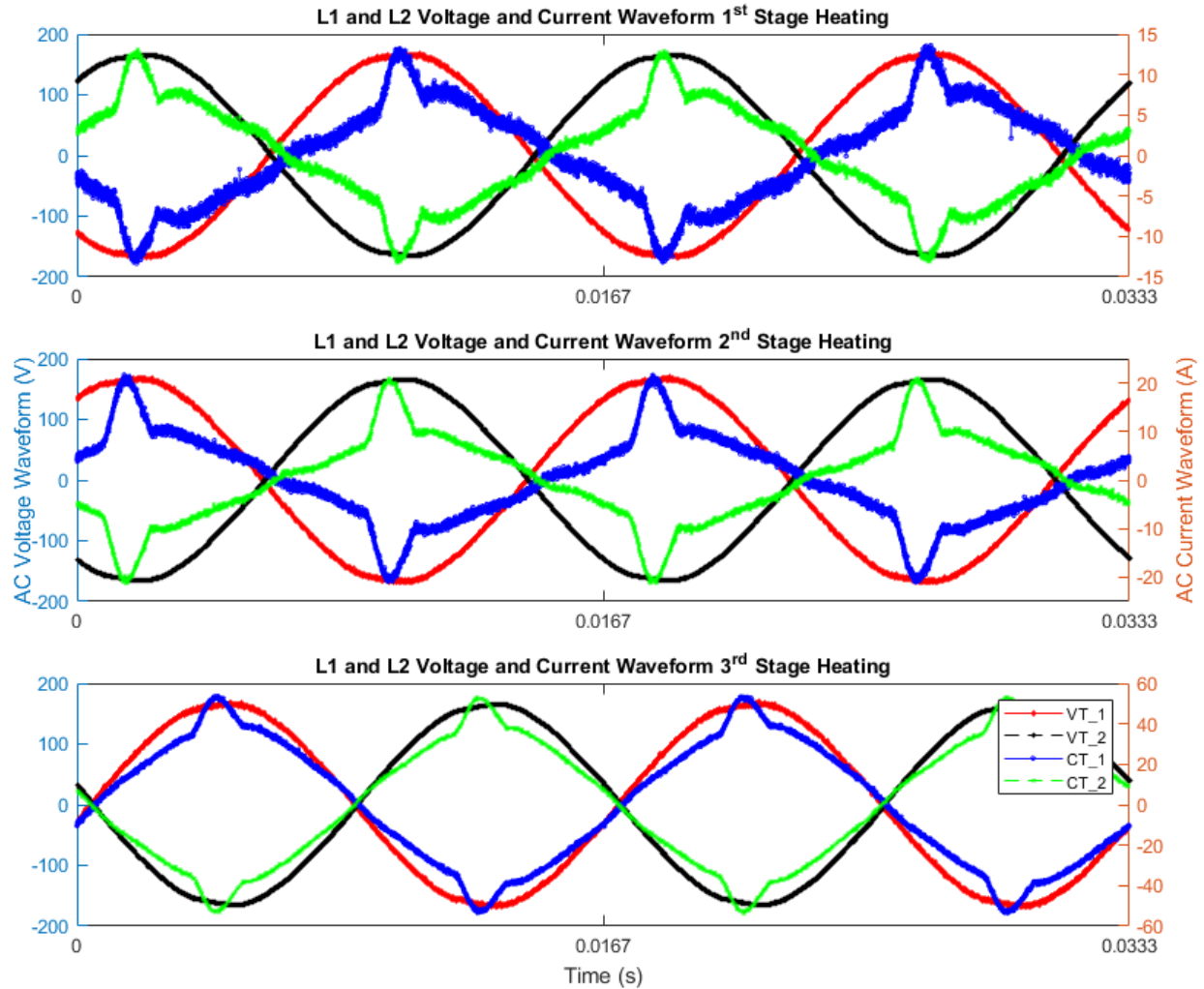
Fig. 3. The voltage and current characteristics of the heat pump waveform in the heating season

As shown in Fig. 3, The voltage and current waveforms between L1 and L2 are 180 degrees out of phase. This phase shift is due to the split phase configuration in residential power distribution networks, as the potential difference are measured between lines and the N. The voltage and current consumption of L1 is approximately the mirror image of the voltage and current consumption of L2. The impact of power electronics on the current consumption waveforms is more visible in the 1st Stage and 2nd Stage of operation, compared to the 3rd Stage. In the 3rd Stage, the heat pump relies on a 5 kW auxiliary resistive load to provide heating, reducing the impact of the power electronics on the waveform distortion. Further analysis of power quality associated with the heat pump waveform data is beyond the scope of this document.

Generally, it is difficult and computationally expensive to model the performance of various heat pump components for load analysis and load forecasting using waveform data. A simpler approach for developing load models to conduct stability and load flow analysis is to use the RMS values computed from the waveform data. The RMS amplitude and phase angles of the waveforms measured by CT_1, CT_2, VT_1, and VT_2 sensors on the utility side of the meter were used. The current consumption of the heat pump on the utility side of the meter is the sum of the current

consumption of all individual components of the air-handling and the outdoor units. The Harmonic Parameters Identification algorithm described in [21] was utilized to extract the RMS amplitude and phase angles. The Harmonic Parameters Identification algorithm uses the Hanning window function and interpolated Discrete Fast Fourier Transform to extract the amplitude and phase angles of the voltage and current measurements. Fig. **4** shows the RMS voltage and RMS current consumption of the three stages of the heat pump operating in the heating mode.
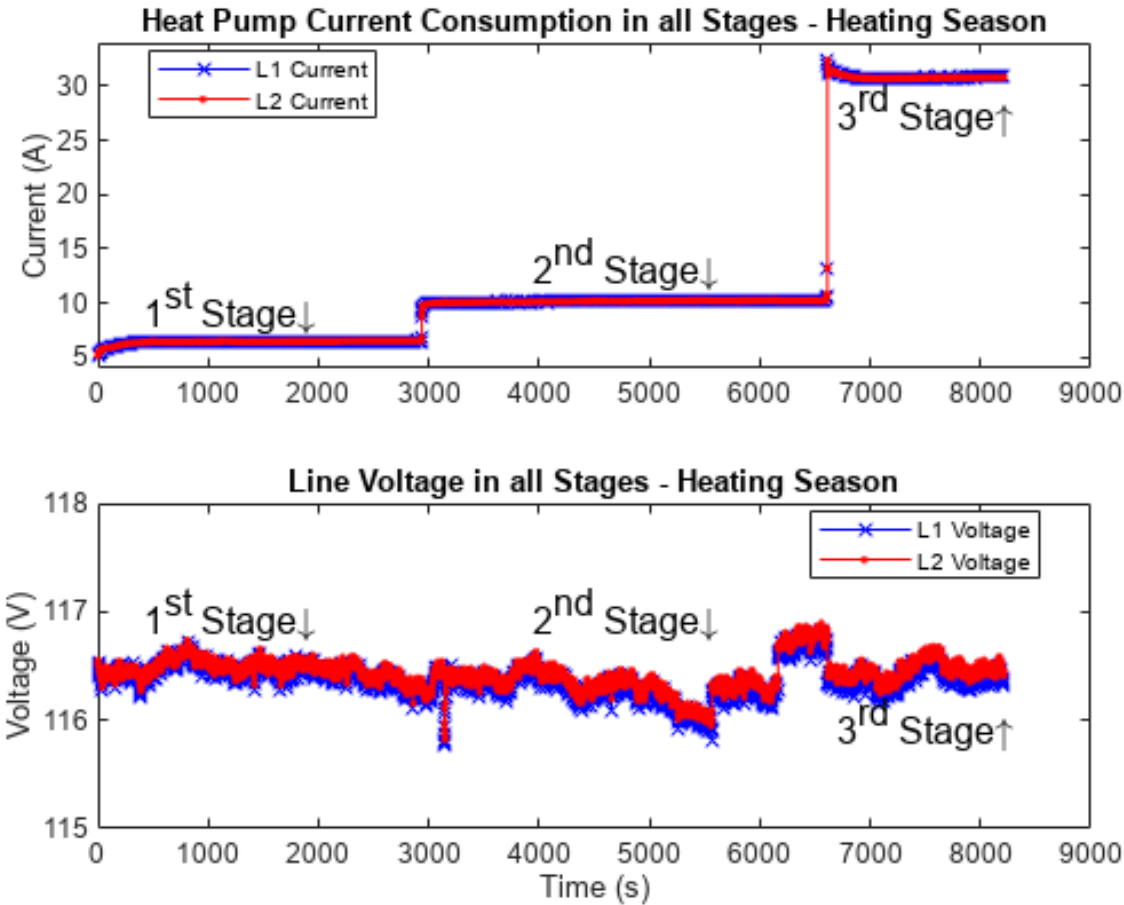
Fig. 4. The RMS values of voltage and current characteristics of the heat pump in the heating season

As shown in Fig. 4, the minimum RMS current consumption is 5.2 A (1st Stage), and the maximum RMS current consumption is 32.5 A (3rd Stage). The current consumption of the heat pump in the 3rd Stage is the sum of the current consumption of the 2nd Stage, and the current consumption resulted from activating a 5 kW resistive load. The minimum RMS voltage is 115.8 V, and the maximum RMS voltage is 116.9 V.

Fig. **5** shows the RMS voltage and RMS current consumption for the two stages of the heat pump operating in the cooling season. In the cooling season, immediately after the 1st Stage is activated, the magnitude of the inrush current reaches approximately 44 A, lasting only 1 s. The inrush current is not shown in Fig. 5. The inrush current was not included in the heat pump modeling process because it severely diminished the accuracy of the LA discussed in Sec. 4.1.
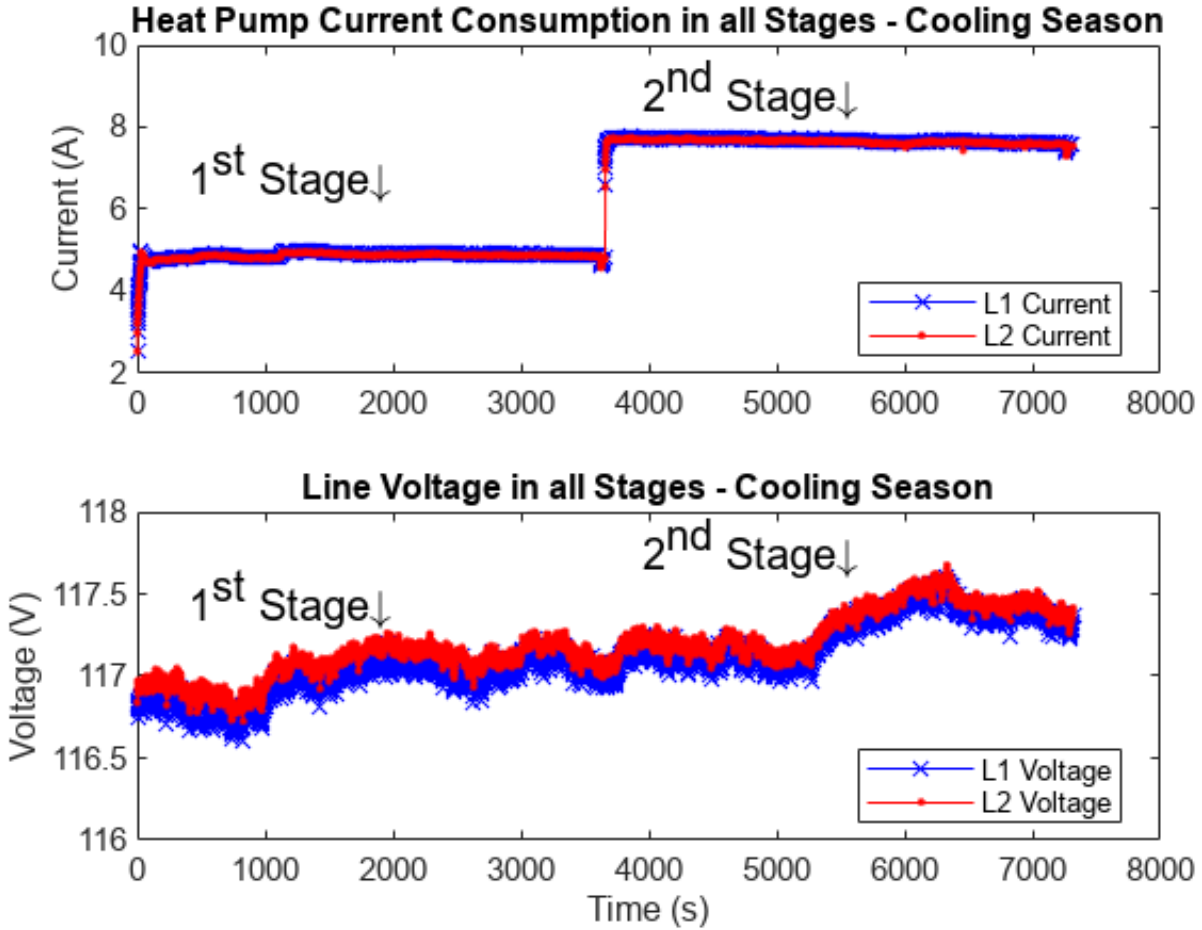
Fig. 5. The RMS values of voltage and current characteristics of the heat pump in the cooling season

As shown in Fig. 5, the minimum RMS current consumption is 2.5 A (1st Stage), and the maximum RMS current consumption is 7.8 A (2nd Stage). The minimum RMS voltage is 116.6 V, and the maximum RMS voltage is 117.7 V. The RMS values shown in Fig. 4 and Fig. 5 were used to develop the data-driven RL Model to predict the current consumption of the two-stage heat pump in heating and cooling seasons.

3. Resistor-Inductor (RL) Model

Consider a simple first-order RL circuit where the resistor R and inductor L elements are in series with each other. The voltage drop across the first-order RL circuit is given by

$$-V_s(t) + i_L(t)R + V_L(t) = 0, \tag{1.1}$$

where, $V_s(t)$ is the source voltage (V), $i_L(t)$ is the inductor current (A), R is the resistor (Ω), and $V_L(t)$ is the voltage across the inductor element (V). The differential form of Eq. (1.1) is given by

$$-V_s(t) + i_L(t)R + L\frac{di}{dt} = 0$$

$$\frac{di}{dt} = \frac{V_s(t)}{L} - i_L(t)\frac{R}{L},$$

(1.2)

where, the voltage across the inductor is $V_L(t) = L\frac{di}{dt}$. The integration form of Eq. (1.2) is given by

$$\int_{i_L(t_0)}^{i_L(t)} \frac{di}{\left(i_L(t) - \frac{V_s(t)}{R}\right)} = \int_{t_0}^{t} \frac{-R}{L} dt.$$

(1.3)

Integrating Eq. (1.3) and solving for $i_L(t)$ provides the time dependent inductor current across the RL circuit given by

$$i_L(t) = \left(i_L(t_0) - \frac{V_s(t)}{R}\right) e^{-\frac{R}{L}(t-t_0)} + \frac{V_s(t)}{R}.$$

(1.4)

The inductor current described by Eq. (1.4) has a transient component and a steady-state term. The transient component is shown in Eq. (1.5),

$$\left(i_L(t_0) - \frac{V_s(t)}{R}\right) e^{-\frac{R}{L}(t-t_0)}.$$

(1.5)

After some time has elapsed the transient part of Eq. (1.4) decays and the current consumption is dominated by the stead-state term of Eq. (1.4). The steady state current ($I_L(t)$) is given in Eq. (1.6),

$$I_L(t) = \frac{V_s(t)}{R}.$$

(1.6)

In a typical energy analysis approach, the steady-state power consumption of a heat pump is linearly dependent on the outdoor temperature [11, 22]. Consequently, the instantaneous steady-state power consumption of the heat pump is expressed as a first-order linear model

$$P_{hp}(t) = m \times T_\infty(t) + b,$$

(1.7)

where, m is the slope of the linear model (W/°C), $T_\infty(t)$ is the outdoor dry bulb temperature (°C), and b is the intercept (W). Alternatively, the instantaneous power consumption of an electrical circuit can be calculated by

$$P = V_{rms} \times I_{rms} \times \cos(\theta),$$

(1.8)

where, $\cos(\theta)$ is the displacement power factor. Substituting $I_L(t)$ for I_{rms} and $V_s(t)$ for V_{rms} in Eq. (1.8) give us

$$P_L(t) = V_s(t) \times I_L(t) \times \cos(\theta). \tag{1.9}$$

$P_L(t)$ is the time dependent (at each time step) instantaneous steady-state power consumption as function of the source voltage $V_s(t)$ and steady-state current consumption of the RL circuit.

Assuming a unity power factor and neglecting the impact of the distortion power factor, solving Eq. (1.9) for the steady-state current $I_L(t)$ give us the following relationship

$$I_L(t) = \frac{P_L(t)}{V_s(t)}. \tag{1.10}$$

Furthermore, substituting $P_{hp}(t)$ (given in Eq. (1.7)) for the value of $P_L(t)$ (given in Eq. (1.10)) enable us to express the steady-state current consumption of the heat pump as a function of $T_\infty(t)$ and line voltage $V_s(t)$. The updated steady-state current consumption, considering the temperature dependency of the heat pump's power consumption, is given by

$$I_L(t) = \frac{P_{hp}(t)}{V_s(t)} = \frac{m \times T_\infty(t) + b}{V_s(t)}. \tag{1.11}$$

The objective is to derive a mathematical expression for capturing the current consumption of each stage of the two-stage heat pump not only as a function of the voltage and displacement power factor but also as a function of the outdoor temperature. Let's assume that Eq. (1.4) provides the foundation for this mathematical expression to predict the heat pump current consumption. Substituting Eq. (1.11) into the steady-state term of Eq. (1.4) give us

$$i_L(t) = \left(i_L(t_0) - \frac{V_s(t)}{R} \right) e^{-\frac{R}{L}(t-t_0)} + \frac{m \times T_\infty(t) + b}{V_s(t)}. \tag{1.12}$$

If the assumption about Eq. (1.4) holds true, then Eq. (1.12) can model the voltage and outdoor temperature dependent performance of the heat pump in both transient and steady-state conditions.

Let $\tau = L/R$ represent the overall time constant (in seconds) of a particular stage of the heat pump, then Eq. (1.12) can be written as

$$i_L(t) = \left(i_L(t_0) - \frac{V_s(t)}{R} \right) e^{-\frac{(t-t_0)}{\tau}} + \frac{m \times T_\infty(t) + b}{V_s(t)}. \tag{1.13}$$

The value of τ (s) in Eq. (1.13) is the time it takes for a particular stage of the heat pump to reach its steady-state current consumption. Understanding the value of τ is a critical information for analyzing the aggregated effect of controlling many heat pumps, as flexible loads, on grid stability and provision of ancillary services. The larger the value of the τ, the slower the response of the

heat pump would be in reaching its steady-state current consumption. Consequently, the values of real and reactive power consumptions, reaching their steady state, reflect the influence of τ. Using Eq. (1.13) to predict the heat pump current consumption requires a data-driven approach because certain parameters must be estimated from measurement data.

The values of $V_s(t)$ and $T_\infty(t)$ are known from measurement for all $t = 1, 2, \dots, T$ (s), where T is the length of time in seconds equivalent to the number of measured data points, assuming each data point is 1 s. However, the values of $R, L, m, and\ b$ are not known a priori. A learning algorithm (LA) is used to estimate these values from measured data. In this paper these unknown values are denoted as effective quantities (R_e, L_e, m_e, b_e) because they are a lumped approximation of the true behavior of the heat pump equipment. These approximations will enable us to predict the current consumption of the heat pump.

A discrete form of Eq. (1.13) is developed by defining $t - t_0$ as $\Delta t = t_{k+1} - t_k$ where $\mathrm{k} = 0, 1, 2, \dots, \mathrm{n}$ are the discrete time steps and n is the number of data points. Let $i_L(k)$ represent the discrete current consumption, the one-step learning and current prediction model is

$$i_{L,k+1} = \left(i_{L,k} - \frac{V_{s,k}}{R_e} \right) e^{-\frac{\Delta t}{\tau_e}} + \frac{m_e \times T_{\infty,k} + b_e}{V_{s,k}}, \qquad (1.14)$$

where $\tau_e = {L_e}/{R_e}$ in (s) is the effective time constant.

4. Learning and Forecasting Schema

The task of developing a data-driven model to predict the current consumption of the heat pump is separated into learning and forecasting components. Fig. **6** shows a schematic representation of the data flows through the learning and forecasting components, leading to predicting power demand. As shown in Fig. 6, the RL Model given by Eq. (1.14) is common to both the Learning Component and the Forecasting Component. The Learning Component is utilized to learn effective parameters of the RL Model, representing various operating stages of the heat pump in both heating and cooling seasons. Using these effective parameters, the Forecasting Component is utilized to predict the current consumption and, ultimately, the power demand of the heat pump in various operating stages and different seasons.
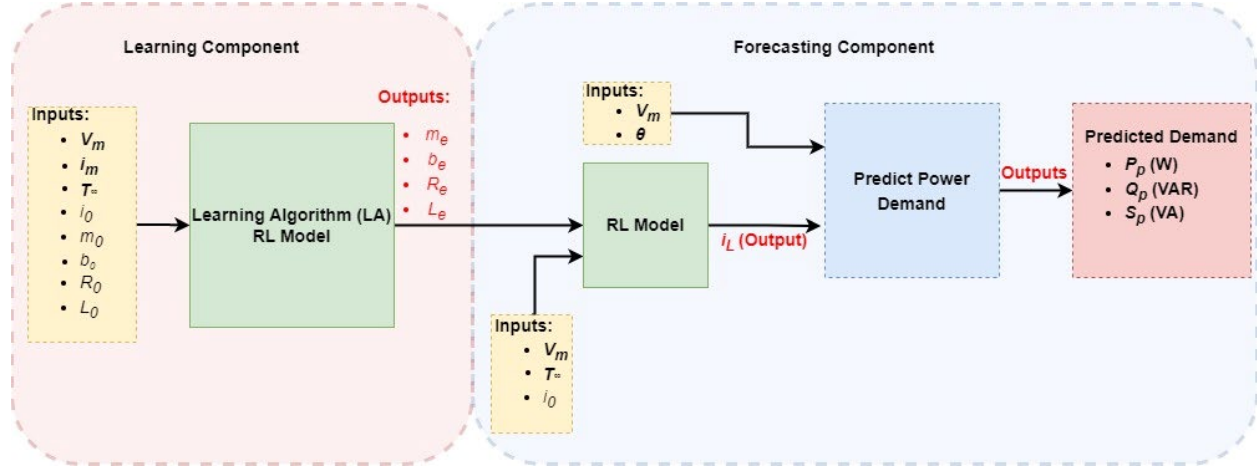
Fig. 6. A schematic representation of the Learning Component and Forecasting Component utilized to learn effective parameters and predict power consumption demand

As shown in Fig. 6, the learning algorithm (LA) utilizes a set of inputs described in Table 2 to estimate the values of the effective parameters m_e, b_e, R_e, and L_e. The LA estimates these effective parameters by reducing the error between the output of the RL Model and the measured RMS current consumption of the heat pump i_m. The Forecasting Component utilizes these effective parameters, the measured RMS voltage V_m, outdoor temperature T_∞, and the initial starting point i_0 to predict the current consumption of the heat pump i_L. Similarly, using i_L, V_m, and the phase angle difference between the voltage and current waveforms θ, the Forecasting Component predicts the real (P_p), reactive (Q_p), and apparent power (S_p) demand of the heat pump. The modular approach between learning and forecasting enables us to test the LA with new data sets and evaluate the impact of the changes in voltage and outdoor temperature on predicting load demand.

Table 2. List of Inputs Used in the Learning and Forecasting Methodologies

Inputs	Description
V_m	A vector of RMS voltage calculated from measured voltage waveform $V_s(t)$ in every second (V). The RMS voltages for the heating and cooling seasons are shown in the bottom images of Fig. 4 and Fig. 5, respectively.
i_m	A vector of RMS current calculated from measured current waveform $i_L(t)$ in every second (A). The RMS current for the heating and cooling seasons are shown in the top images of Fig. 4 and Fig. 5, respectively.
T_∞	A vector of the outdoor dry bulb temperature in every second obtained from interpolating minutely measured outdoor temperature data (°C).
i_0	Initial current value obtained from $i_m(0)$ (A)
m_0	Initial value of the slope of the linear model given in Eq. (1.7) (W/°C)
b_0	Initial value of the intercept of the linear model given in Eq. (1.7) (W)
R_0	Initial value of the resistor in the RL Model calculated by dividing $\dfrac{V_m(0)}{i_m(0)}$ (Ω)
L_0	Initial value of the inductor, arbitrary selected (H)
θ	A vector of the phase angle differences between the voltage and current waveforms computed every second $\theta = (\theta_v - \theta_i)$ (rad)

The initial values of i_0, R_0, L_0, m_0, and b_0 are given in Table 3. The mechanism for obtaining the values of i_0, R_0, and L_0 were provided in Table 2. The initial values for m_0, and b_0, describing the slope and intercept of Eq. (1.7) were obtained from performance of the two-stage air-source heat pump in the NZERTF [23].

Table 3. Initial Values of Current and Effective Parameters Used in LA

Phase	Season	Stages	$i_0(A)$	$R_0(\Omega)$	$L_0(H)$	$m_0(W/°C)$	$b_0(W)$
L1-N & L2-N	**Heat**	**1st Stage**	5.2	22.6	1.0E-06	7.0	1096.8
		2nd Stage	6.5	17.8	1.0E-06	6.7	1747.6
		3rd Stage	32.5	3.6	1.0E-06	6.7	1747.6
	Cool	**1st Stage**	2.5	45.9	1.0E-06	16.3	-105.0
		2nd Stage	4.8	24.2	1.0E-06	19.3	438.6

4.1. The Learning Algorithm (LA)

To predict i_L, the effective parameters τ_e, m_e, and b_e of the RL Model, given by Eq. (1.14), were estimated using a curve fitting optimization technique. The objective function of the LA was defined as least-squares error (l_2 norm) between the measured current consumption of the heat pump (i_m) and the predicted current (i_L). The objective function is given by

$$f(R_e, L_e, m_e, b_e) = \|i_m - i_L\|_2, \text{ and} \tag{1.15}$$

the optimization problem is

$$\min_{R_e, L_e, m_e, b_e} f(R_e, L_e, m_e, b_e)$$
$$lb \leq R_e \leq ub$$
$$lb \leq L_e \leq ub$$
$$lb \leq m_e \leq ub \tag{1.16}$$
$$lb \leq b_e \leq ub,$$

where, all effective parameters are constrained within a lower $lb = 1e - 6$ and upper bounds of $ub = 1e5$. The choices for lb and ub were arbitrary selected for numerical convergence and stability.

The choice of initial values (starting points) for the effective parameters m_e, b_e, R_e, and L_e could significantly impact the LA performance and the RL Model's output quality. These choices affect the convergence of the LA to an optimum solution because the function given in Eq. (1.16) can have multiple local minimum values satisfying the non-linear objective function given in Eq. (1.15). To address these issues, the MATLAB's MultiStart optimization algorithm was used to evaluate up to fifty randomly generated starting points. For reproducibility of random numbers, the random number generator in the MATLAB R2022b release was set to its default settings (`rng default`). In the MultiStart routine, the `fmincon` algorithm was selected as the local solver.

The local solver algorithm was prevented from evaluating infeasible starting points by setting the `StartPointsToRun` option of MultiStart algorithm to `bounds`.

The prediction capability of the LA for modeling the current consumption of the two-stage heat pump, three cases shown in Fig. 7, Fig. 8, and Fig. 9 were selected. These cases provide a comparison between the measured (i_m) and predicted (i_L) current consumption of the heat pump for the 1st Stage, 2nd Stage, and 3rd Stage of heating. All cases include the plot for L1 and L2 phases in the heating season. The current consumption on L1 and L2 were measured at nominal 116 V AC. The LA minimized the least-squares differences (l_2 norm) between the output of the model and the measured current values. To evaluate the merit of the RL Model, the root mean square error (RMSE) statistical method was used. The RMSE of individual fit for each stage of the heat pump and L1 and L2 phases are reported in their respective plots.
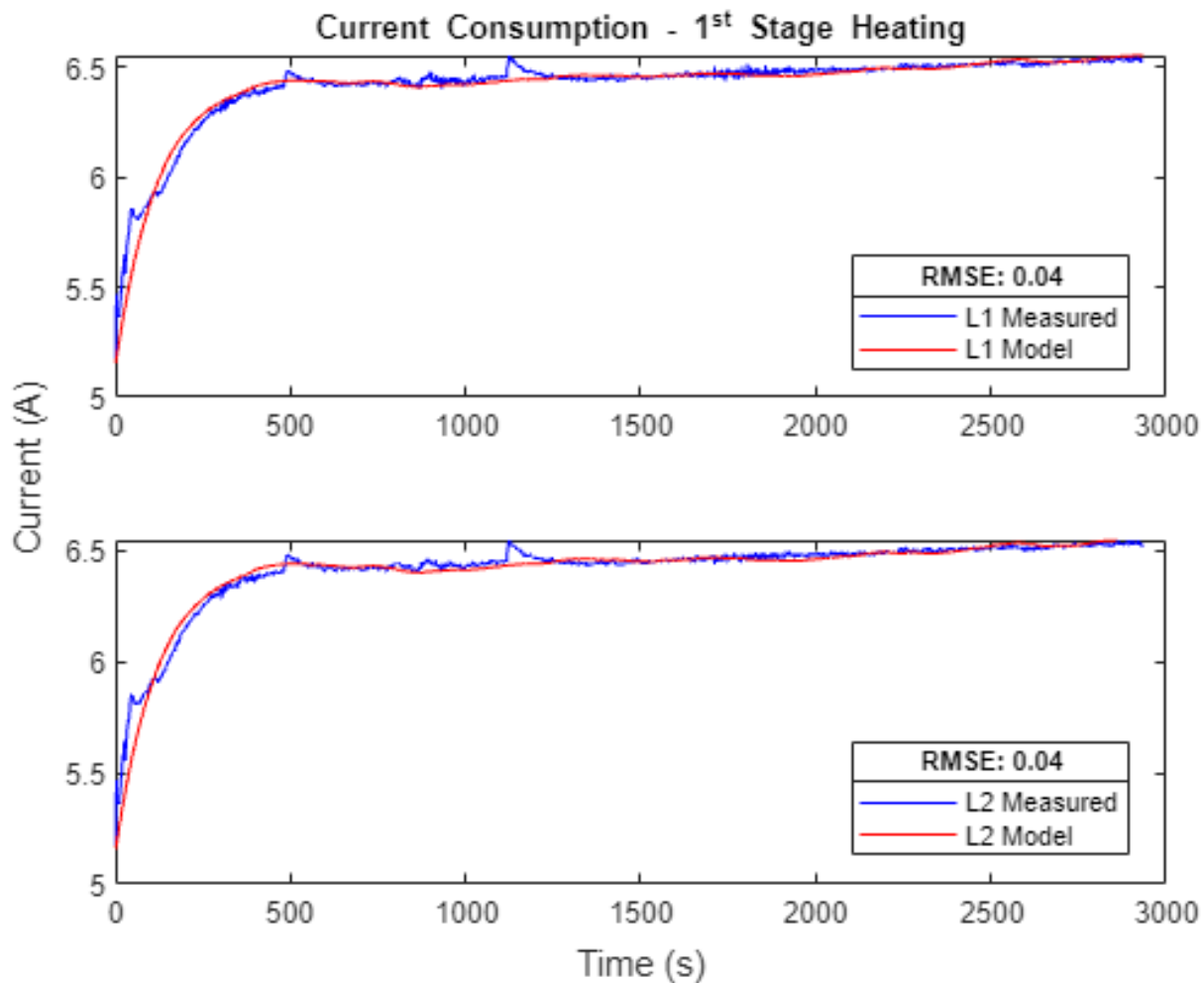
Fig. 7. Measured versus predicted current consumption of the heat pump on L1 and L2 phases during the 1st Stage of heating

As shown in Fig. 7, the heat pump's response to reach 63.2 % of its steady-state current consumption in 125 s given by the effective time constant τ_e in Table 4. In inductive or capacitive loads, five-time constants ($5\tau_e$) provide a good approximation for reaching within 1 % of the

steady-state value of the circuits. In contrast, the effective time constant τ_e for the 2nd Stage, shown in Fig. 8, is 3 s. In this study, the 2nd Stage of the heat pump was activated while the heat pump was already operating in its 1st Stage as shown in the top plot of Fig. 4.
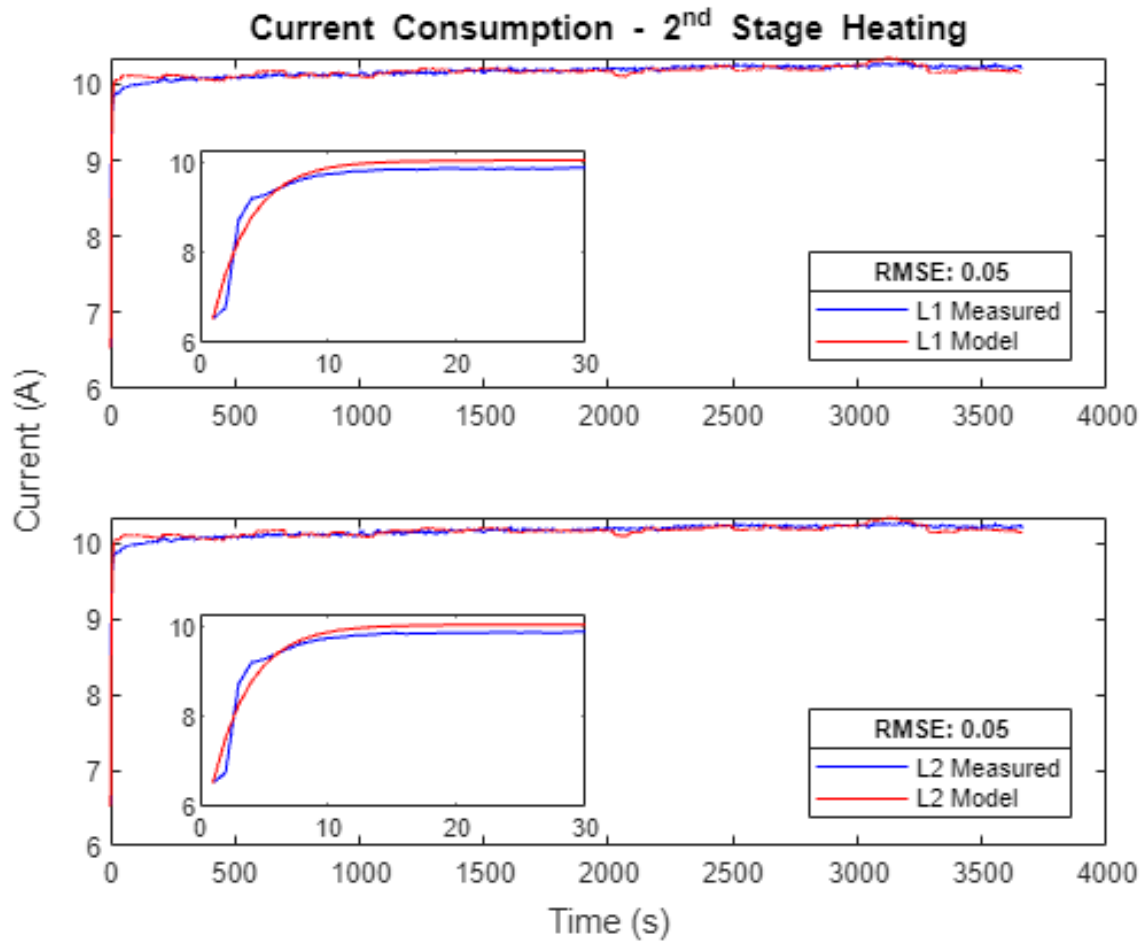
Fig. 8. Measured versus predicted current consumption of the heat pump on L1 and L2 phases during the 2nd Stage of heating

As shown in Fig. 7 and Fig. 8, there are good agreements between the measured current consumption and predicted current consumption in both transient and steady-state conditions. For visual clarity, embedded subplots in Fig. 7 show the first 30 s of the heat pump's current consumption in the 2nd Stage of operation.
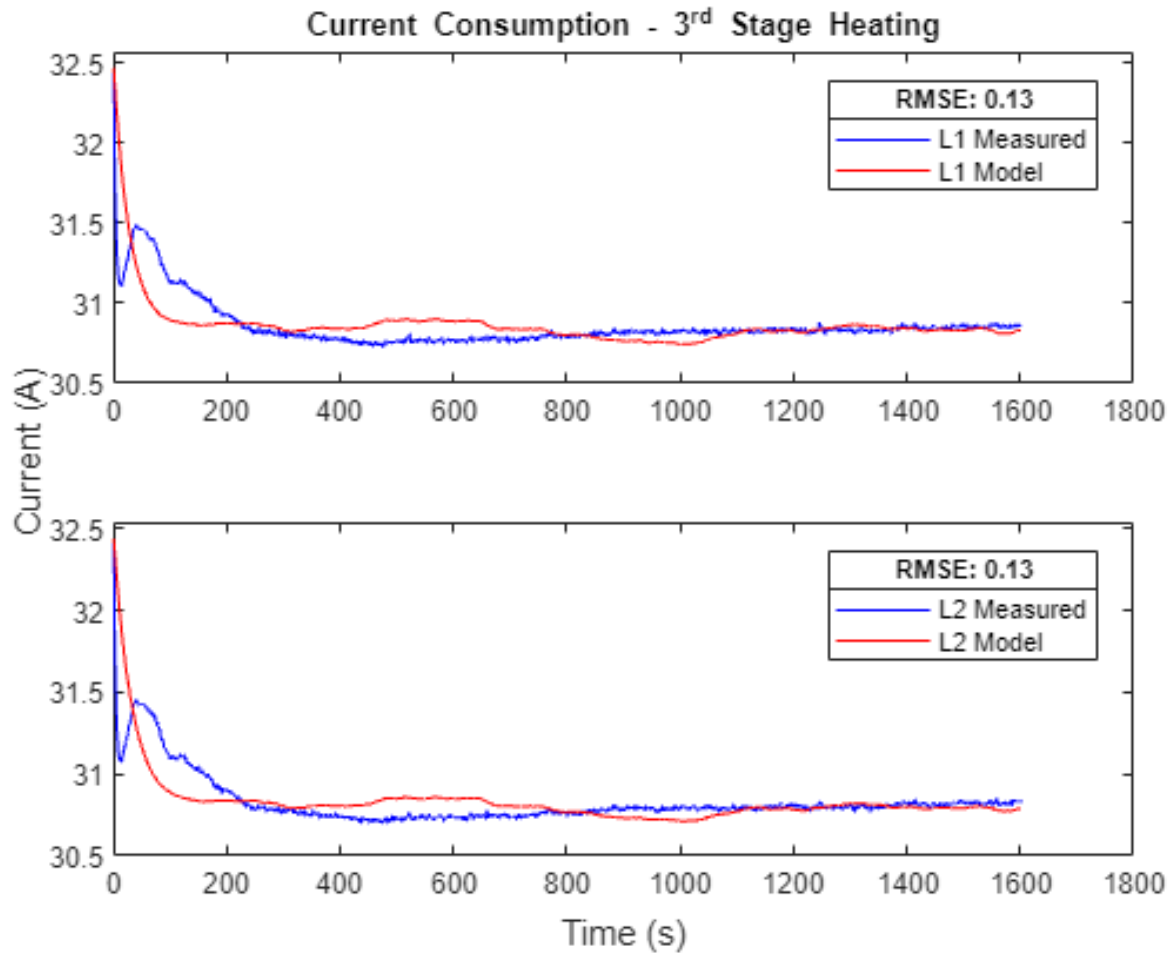
Fig. 9. Measured versus predicted current consumption of the heat pump on L1 and L2 phases during the 3rd Stage of heating

In contrast to Fig. 7 and Fig. 8, the transient behavior of the heat pump operating in the 3rd Stage exhibits an exponential decay, as shown in Fig. 9. The effective time constant τ_e in the 3rd Stage is 28 s. As shown in Fig. 9, the RL Model cannot capture the exact behavior of the heat pump during the transient period; however, it provides a good approximation for the current consumption as validated by the lower values of RMSE. The 3rd Stage of the heat pump was activated while the heat pump was already operating in its 2nd Stage as shown in the top plot of Fig. 4.

The prediction capability of the LA for modeling the current consumption of the two-stage heat pump during the cooling season exhibits similar patterns and low RMSE values, as shown in Fig. 7, Fig. 8, and Fig. 9 for the heating season. The plots for the 1st Stage and 2nd Stage operating of the heat pump in the cooling season are shown in Appendix A of this document. A summary of estimating effective parameters, time constants, and RMSE values for all modeling activities in this study are provided in Table 4.

4.1.1. Estimated Effective Parameters, Time Constants, and RMSE

Application of the LA resulted in a set of effective parameters for the RL Model, representing all stages of operation and various seasons. A summary of effective parameters and the calculated time constants for each stage of the heat pump is shown in Table 4. Table 4 also shows the calculated values of RMSE between measured and predicted values.

Table 4. The Values of Effective Parameters, Time Constants, and RMSE, Resulting from the Application of the LA

Phase	Season	Stages	$R_e(\Omega)$	$L_e(\text{H})$	$m_e(W/{^\circ}C)$	$b_e(W)$	$\tau_e(s)$	RMSE
L1-N	Heat	1st Stage	727.8	90817.0	0.1	23.4	124.8	0.04
		2nd Stage	5096.8	14984.4	6.9	194.5	2.9	0.05
		3rd Stage	199.3	5570.8	0.0	191.7	28.0	0.13
	Cool	1st Stage	8598.9	99992.1	0.0	48.6	11.6	0.05
		2nd Stage	29.5	45.2	13.7	373.6	1.5	0.03
L2-N	Heat	1st Stage	617.4	78434.3	0.1	26.6	127.0	0.04
		2nd Stage	5215.1	15307.2	7.0	192.8	2.9	0.05
		3rd Stage	267.2	8713.2	0.0	157.5	32.6	0.13
	Cool	1st Stage	8728.1	99991.4	0.0	49.1	11.5	0.05
		2nd Stage	26.4	40.5	13.7	401.5	1.5	0.03

4.2. Predicting Real and Reactive Power Consumption

The equations for calculating the real power (active power) and reactive power consumption of the heat pump are given by

$$P_p = V_m \times i_{m,L} \times \cos(\theta), and$$
$$Q_p = V_m \times i_{m,L} \times \sin(\theta),$$

(1.17)

where:

V_m is the measured RMS voltage (V),
$i_{m,L}$ is the measured current i_m or the predicted current i_L(A),
$\theta = \theta_v - \theta_i$ is the phase angle difference between the voltage and current waveforms (rad). The procedure for obtaining the voltage phase angle θ_v and the current phase angles θ_i were described in Sec. 2.1.,
P_p is the real power (W),
Q_p is the reactive power (VAR).

The Forecasting Component, as shown in Fig. 6, uses i_L in Eq. (1.17) to calculate the predicted real, reactive, and apparent power consumption of the heat pump. Whereas i_m in Eq. (1.17) was used to calculate the measured real and reactive power consumption of the heat pump. The apparent power consumption can be calculated by

$$S_p = \sqrt{(P_p)^2 + (Q_p)^2} \, , \tag{1.18}$$

where, the apparent power S_P is in (VA), and P_P and Q_P are described in Eq. (1.17).
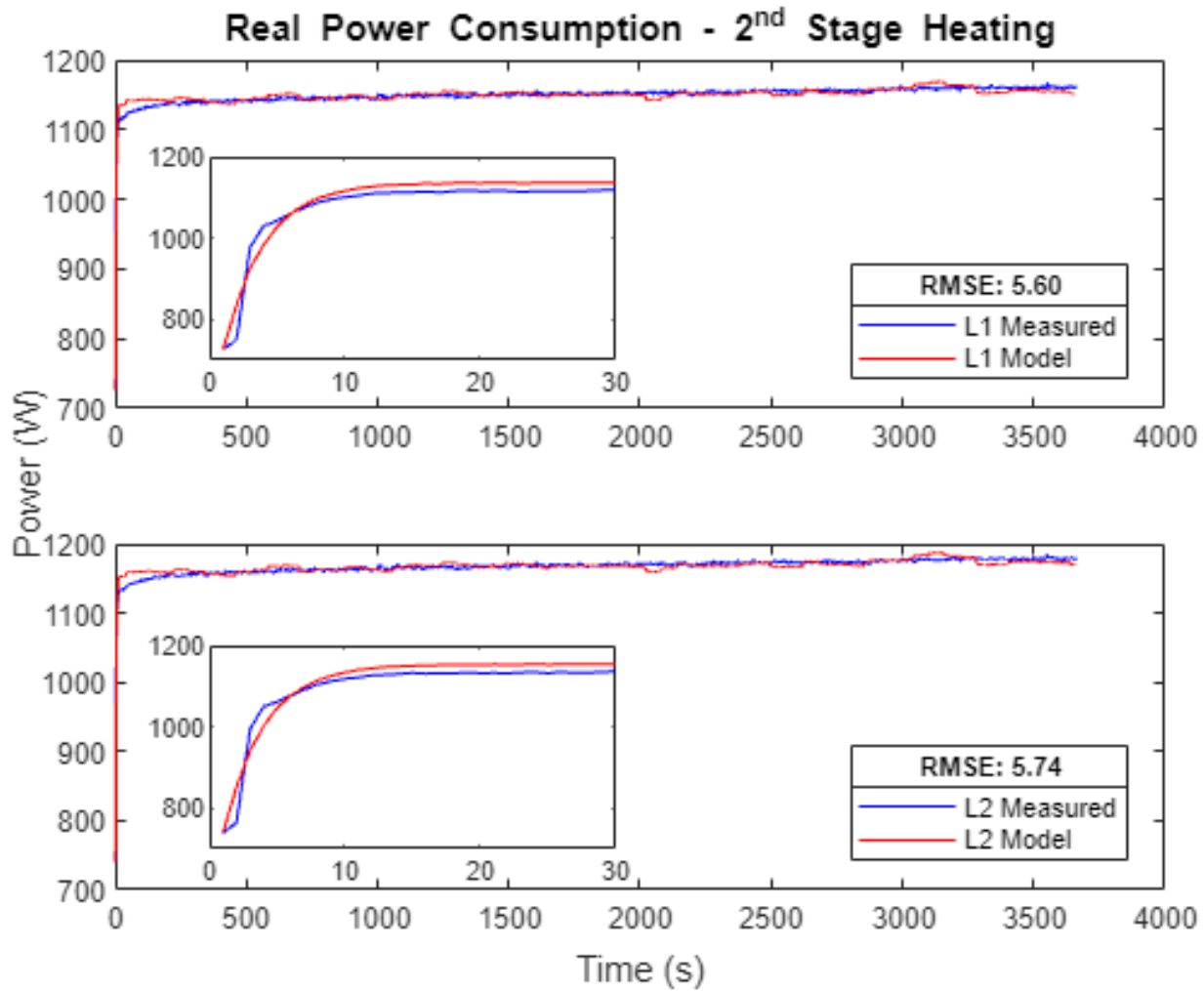
4.2.1. Real Power Consumption

A comparison between the measured and predicted real power consumption of the heat pump during the 1ˢᵗ Stage of heating is shown Fig. 10.
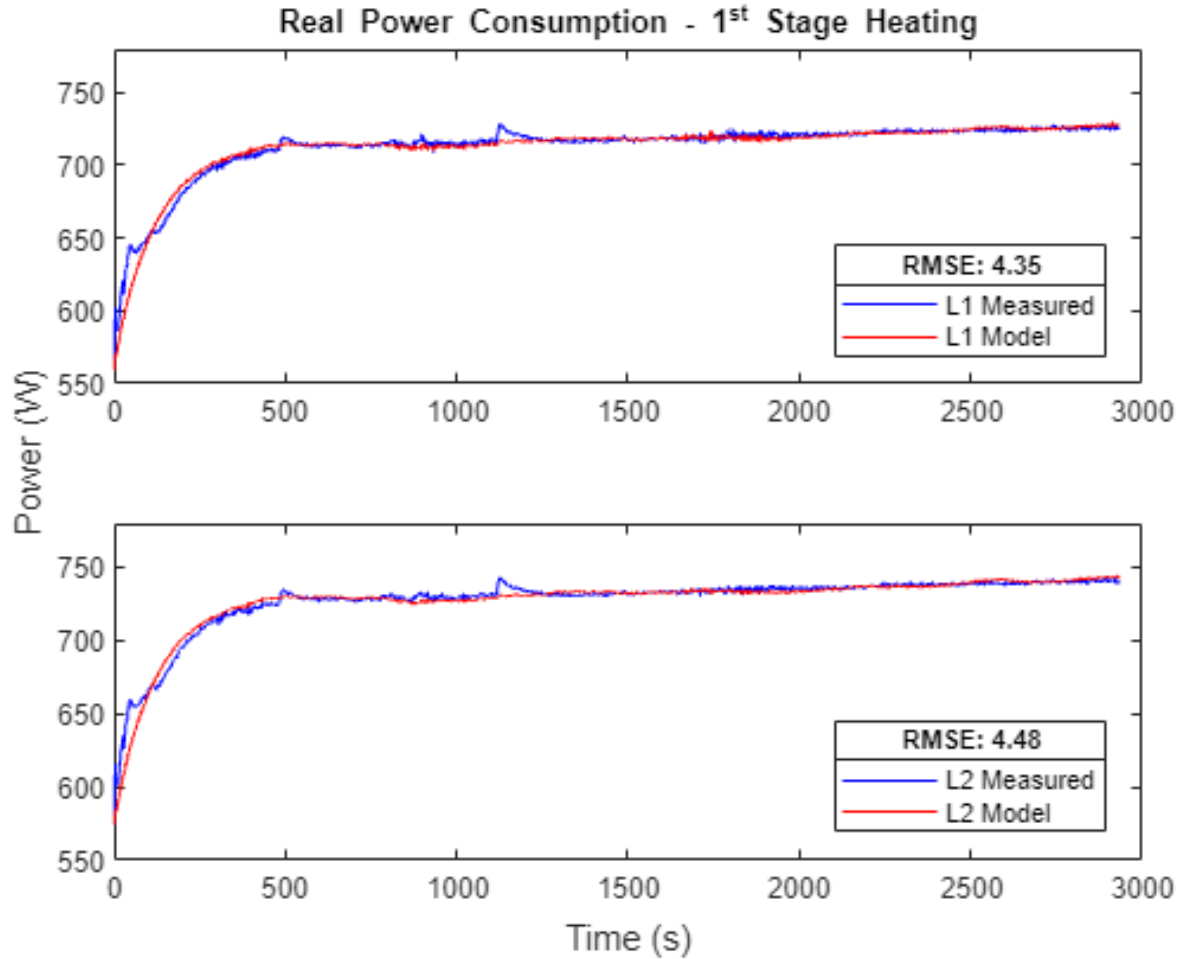
Fig. 10. Measured versus predicted real power consumption (P_p) of the heat pump on L1 and L2 phases during the 1st Stage of heating

As shown in Fig. 10, the predicted real power consumption (P_p) of the 1ˢᵗ Stage of heating closely follows the shape of the current consumption in the 1ˢᵗ Stage of heating, as shown in Fig. 7. The RMSE values for the predicted versus measured P_p is higher than the RMSE values reported in Fig. 7 for the predicted current consumption i_L. This increase in the RMSE values is expected because the output of the RL Model, given by Eq. (1.14), is independent of the phase angle differences and their impact on its forecasting capabilities.
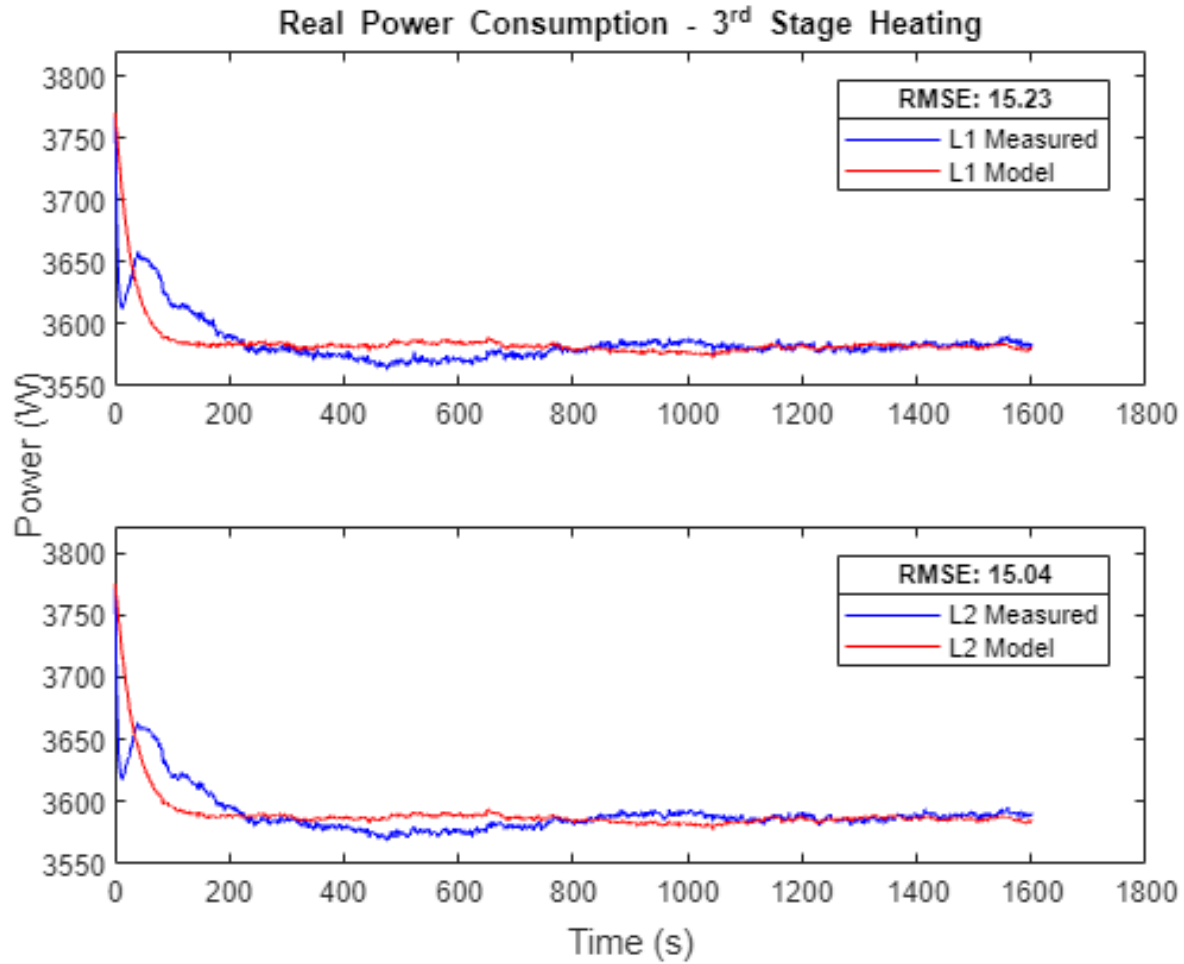
A comparison between the measured and predicted real power consumption of the heat pump during the 2nd Stage of heating is shown Fig. 11.

Fig. 11. Measured versus predicted real power consumption (P_p) of the heat pump on L1 and L2 phases during the 2nd Stage of heating

As shown in Fig. 11, the predicted real power consumption (P_p) of the 2nd Stage of heating also closely follows the shape of the current consumption in the 2nd Stage of heating, as shown in Fig. 8. The RMSE values for the predicted versus measured P_p is higher than the RMSE values reported in Fig. 8 for i_L. For visual clarity, the embedded subplots in Fig. 11 show the first 30 s of the heat pump's power consumption in the 2nd Stage of operation.

A comparison between the measured and predicted real power consumption of the heat pump during the 3rd Stage of heating is shown Fig. 12.

Fig. 12. Measured versus predicted real power consumption (P_p) of the heat pump on L1 and L2 phases during the 3rd Stage of heating

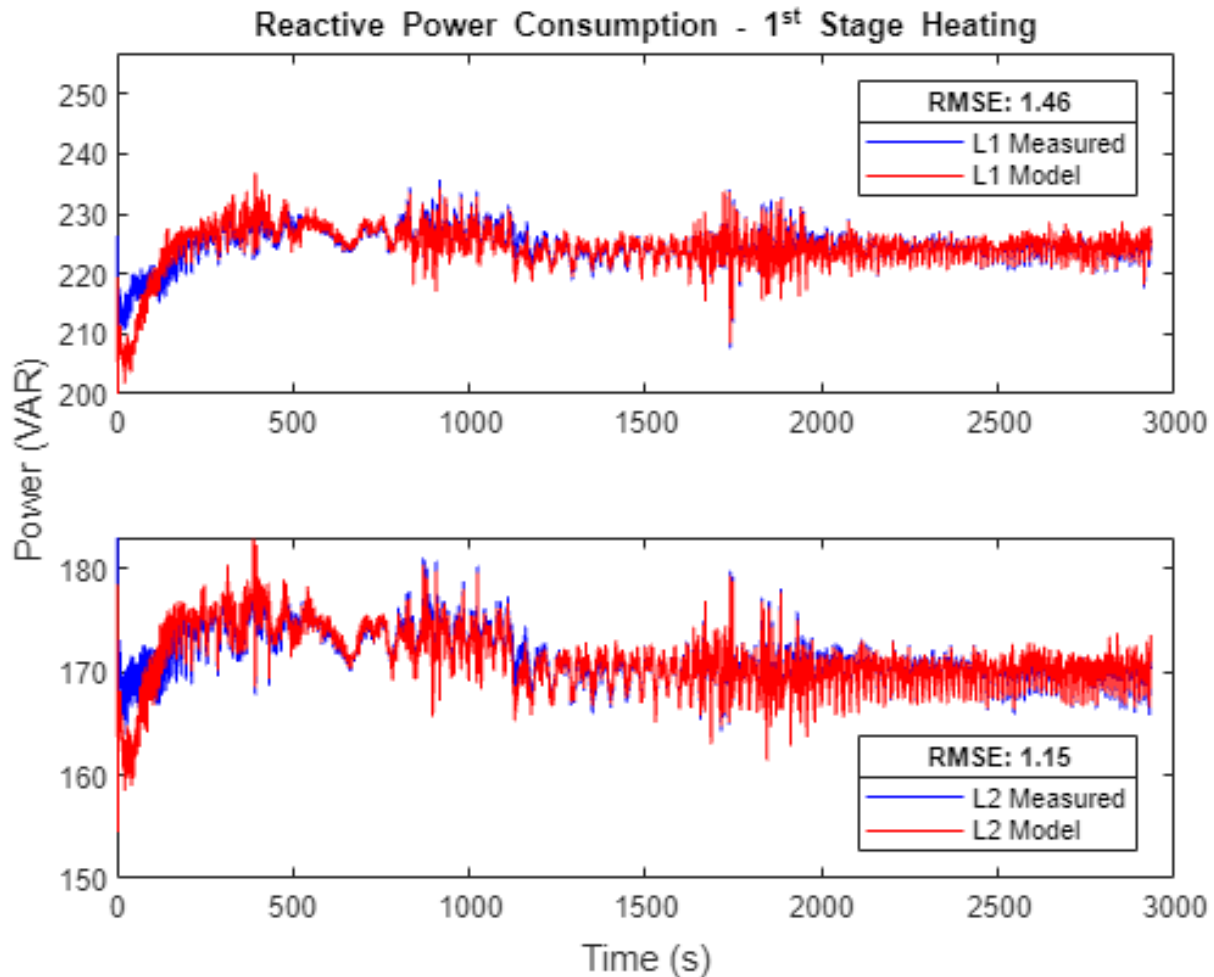As shown in Fig. 12, the predicted real power consumption (P_p) of the 3rd Stage of heating also closely follows the shape of the current consumption in the 3rd Stage of heating, as shown in Fig. 9. The RMSE values for the predicted versus measured P_p is much higher than the RMSE values reported in Fig. 9 for i_L. The RMSE values for the 3rd Stage, as shown in Fig. 12, are approximately three times higher than the RMSE values for the 1st Stage and 2nd Stage of operation. This noticeable increase in the prediction error for 3rd Stage power consumption can be attributed to the limitation of the RL Model in capturing the exact behavior of the heat pump during the transient period and the impact of the phase angle difference θ. In contrast to the 1st Stage and 2nd Stage heating, the initial power consumption of the 3rd Stage is much higher than its steady-state values. The initial transient portion of the 3rd Stage quickly decays to a certain value just above the steady-state power consumption; however, it rises again by a certain value and then starts its slower exponential decay towards the steady-state power consumption.

Knowing the behavior of the transient portion of the heat pump's real power consumption could be consequential for aggregators and system operators looking to develop control strategies for

providing ancillary services. The plots representing the real power consumption of the heat pump in the cooling season are provided in Appendix B of this document.
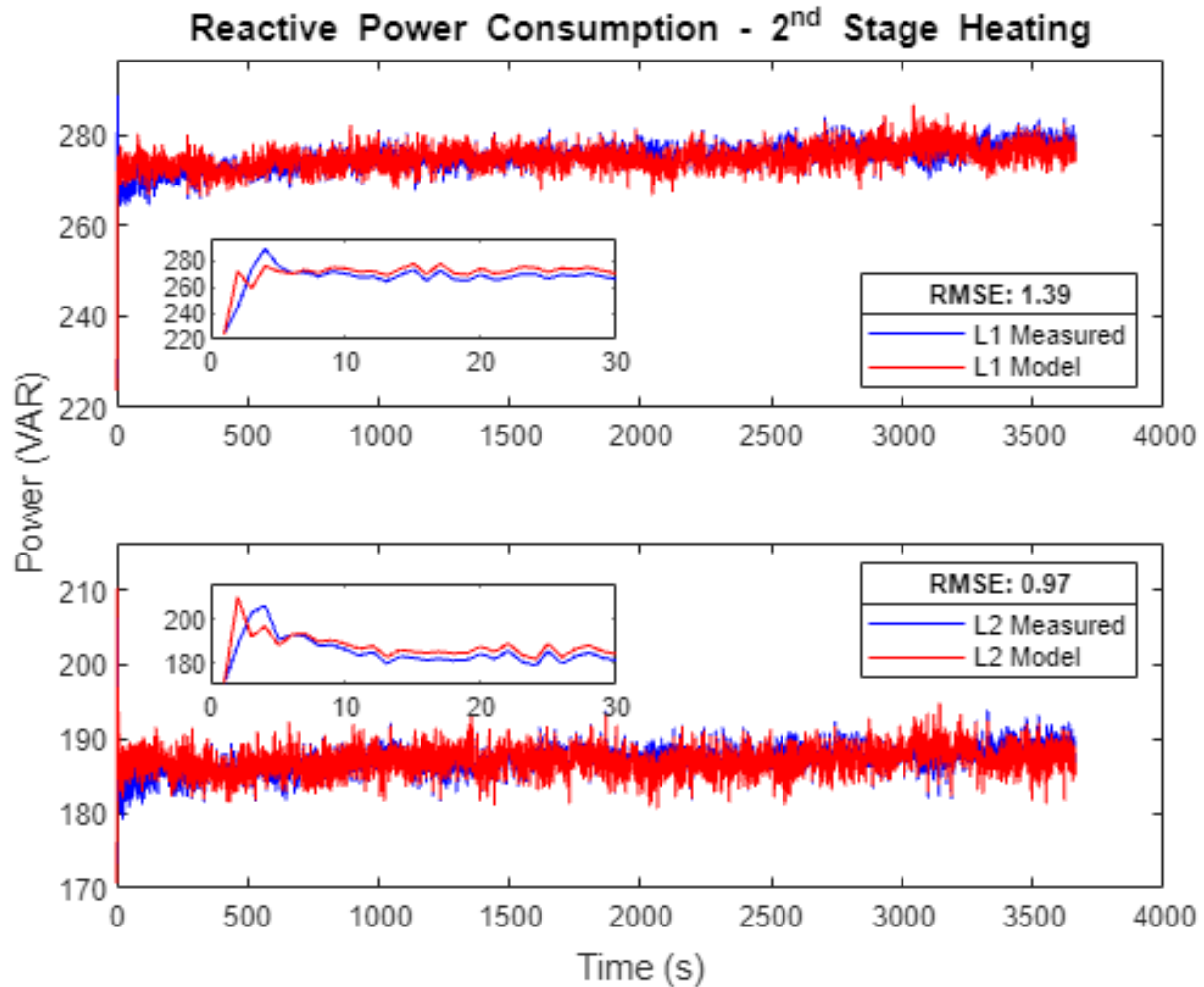
4.2.2. Reactive Power Consumption

A comparison between the measured and predicted reactive power consumption of the heat pump during the 1st Stage of the heating Fig. 13.

Fig. 13. Measured versus predicted reactive power consumption (Q_p) of the heat pump on L1 and L2 phases during the 1st Stage of heating

As shown in Fig. 13, the predicted reactive power consumption closely matches the measured reactive power. The reactive power on L1 and L2 phases exhibit non-linear exponential behavior during the transient part of the 1st Stage operation. The traces in Fig. 13 show more fluctuations than the traces shown for the 1st Stage real power consumption in Sec. 4.2.1. These fluctuations may be due to the rapid charging and discharging of the inductive and capacitive elements of the heat pump.
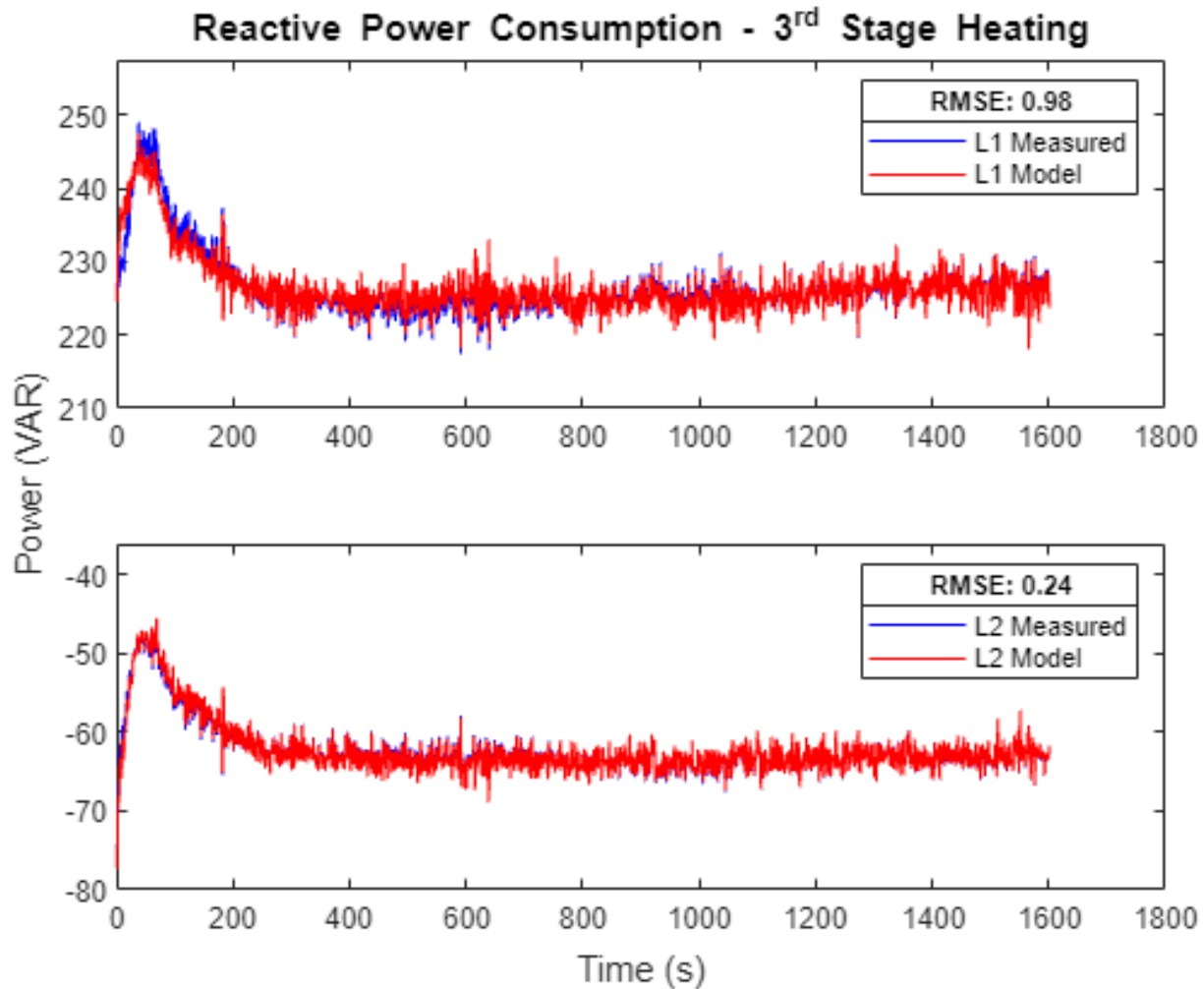
A comparison between the measured and predicted reactive power consumption of the heat pump during the 2nd Stage of heating is shown Fig. 14.

Fig. 14. Measured versus predicted reactive power consumption (Q_p) of the heat pump on L1 and L2 phases during the 2nd Stage of heating

As shown in Fig. 14, the predicted reactive power consumption closely matches the measured reactive power. The reactive power on L1 and L2 phases exhibit non-linear exponential behavior during the transient part of the 2nd Stage operation. The traces in Fig. 14 show more fluctuations than those shown for the 2nd Stage's real power consumption in Sec. 4.2.1.

A comparison between the measured and predicted reactive power consumption of the heat pump during the 3rd Stage of heating is shown Fig. 15.

Fig. 15. Measured versus predicted reactive power consumption (Q_p) of the heat pump on L1 and L2 phases during the 3rd Stage of heating

As shown in Fig. 15, the predicted reactive power consumption closely matches the measured reactive power. The reactive powers on L1 and L2 phases exhibit non-linear exponential behavior during the transient part of the 3rd Stage operation. The traces in Fig. 15 show more fluctuations than the traces shown for the 3rd Stage of real power consumption in Sec. 4.2.1. However, compared to the traces of the reactive power shown in Fig. 13 and Fig. 14, the fluctuations are less pronounced because a significant portion of the heat pump load during the 3rd Stage is a 5 kW resistive load. A major difference between the traces of the reactive power in the 3rd Stage and other stages of the heat pump operation is that the reactive power is negative on L2. A positive reactive power indicates the presence of an inductive load, whereas a negative reactive power is indicative of a capacitive load.

The plots representing the real power consumption of the heat pump in the cooling season are provided in Appendix B of this document.

4.2.3. Discussion on Power Flow

The Institute of Electrical and Electronics Engineers (IEEE) Std 1459-2010 [24] provides the four-quadrant power flow diagram for determining the type of loads and the direction of the power flow from the utilities to customer premises. In the IEEE Std 1459-2010 description of the four-quadrant power flow directions, the power flow from a customer location to the utility is termed *received*. In contrast, the power flow from a utility to the customer premise is termed *delivered*.

Using the IEEE Std 1459-2010 descriptions, the real and reactive power consumption in the 1st Stage and 2nd Stage, on L1 and L2 phases, are positive. Since the real and reactive power are positive values, the power is *delivered* from the utility to the load, and the heat pump unit acts like an inductive load. This observation is correct in both the heating and cooling seasons.

The real and reactive power consumption in the 3rd Stage of heating is positive on L1. However, on L2, the real power is positive, but the reactive power is negative, as shown in the bottom subplot of Fig. 15. When the real power is positive, and the reactive power is negative, the heat pump acts like a capacitive load. In this case, the real power is *delivered* to the customer from the utility, and the reactive power is *received* by the utility. In other words, the heat pump injected reactive power back into the utility grid on L2. However, the assertion that the heat pump acts like a capacitive load on one leg of the split phases could be misleading. The real and reactive power consumption of a split-phase system is additive, as shown in Fig. 16. Therefore, the total real and reactive power is positive, and the heat pump is an inductive load.
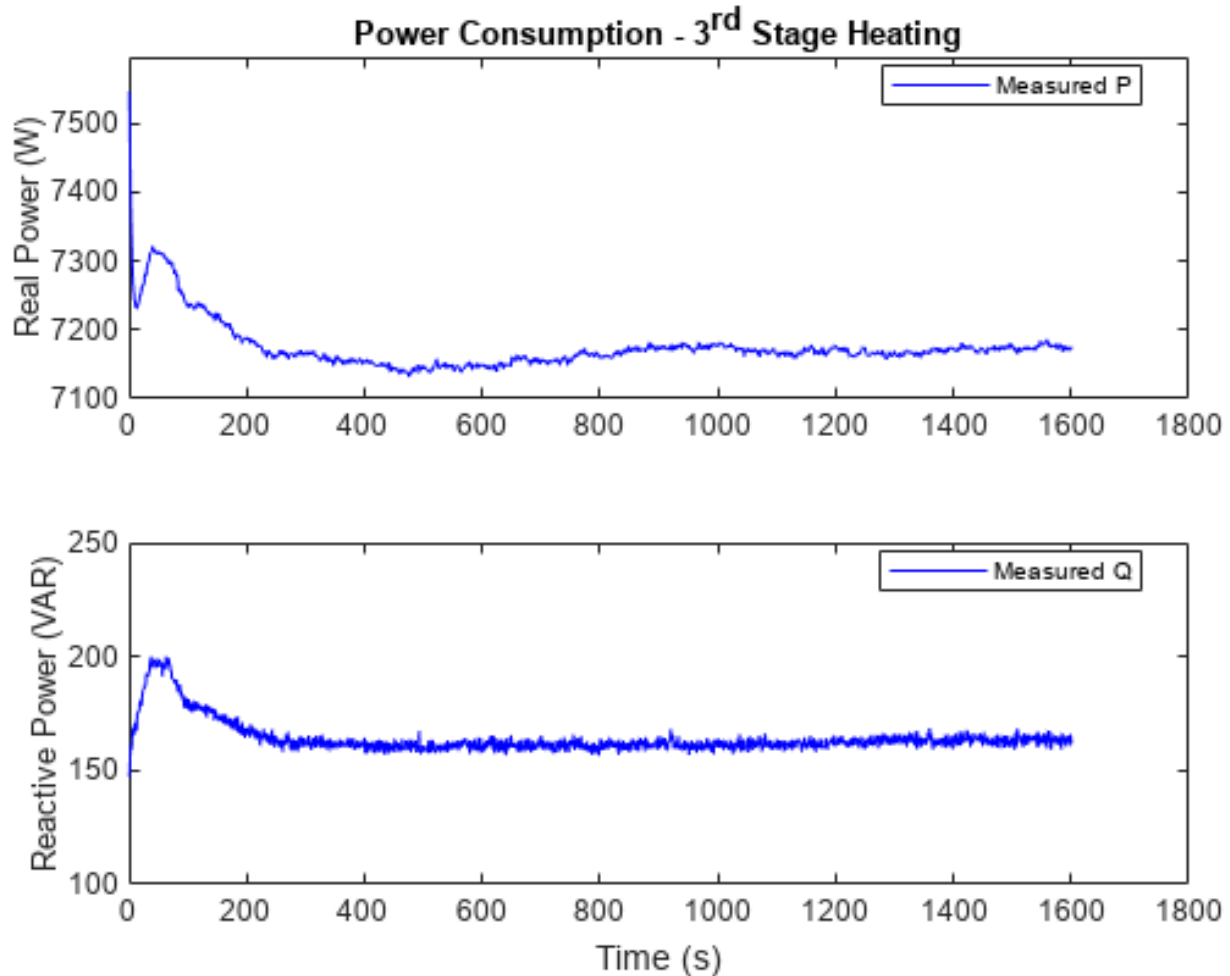
Fig. 16. Measured total real and reactive power consumption of the heat pump during the 3rd Stage of heating

As shown in Fig. 16, the total power consumption of the heat pump is the sum of real and reactive power consumptions on L1 and L2 phases.

5.   Conclusion

Recent work has documented the importance of buildings, as a set of electric loads and generation sources, in managing the stability of the power system in a smart grid. Traditionally, utilities controlled the supply of electric energy to match the demand for buildings to maintain stability. A critical tool for managing the balance between supply and demand is load forecasting. Load forecasting requires models that are accurate, adaptive, and simple to implement. Prior work has documented complicated dynamic models or simplified steady-state modeling approaches for power flow and stability analysis. However, these traditional modeling approaches cannot address the dynamic behavior of the distribution grid that is rapidly changing due to the proliferation of renewable energy sources, electrical storage, including electric vehicles, and non-linear loads such as heat pumps. Heat pumps are a significant source of electric energy consumption in residential buildings. This document demonstrated the development of the novel gray-box model (RL Model) to forecast the two-stage air-source heat pump's steady-state and transient current consumption in

heating and cooling seasons. The RL Model was derived from a solution of a first-order differential equation describing the characteristics of a resistor-inductor equivalent circuit and the steady-state power consumption of a heat pump. Key parameters of the RL Model were estimated using the LA. The performance of the RL Model was validated using measurement data from the Net-Zero Energy Residential Test Facility located on the National Institute of Standards and Technology (NIST) campus in Gaithersburg, MD. The predicted output of the RL Model, current consumption, was used to estimate the heat pump's real and reactive power consumption for different operating stages and seasons. A list of key parameters, like the time constant and temperature-dependent coefficients of the RL Model, were described and tabulated. It was noted that the knowledge of the time constant could provide critical information for analyzing the aggregated effect of controlling many heat pumps, as flexible loads, on grid stability and the provision of ancillary services. The average root mean squared error between the RL Model's predicted current output and the measured current consumption was 0.06.

Appendix A

The following figures depict the prediction capability of the LA for modeling the current consumption of the two-stage heat pump during the cooling season. Each figure shows the comparison between the predicted and measured values.
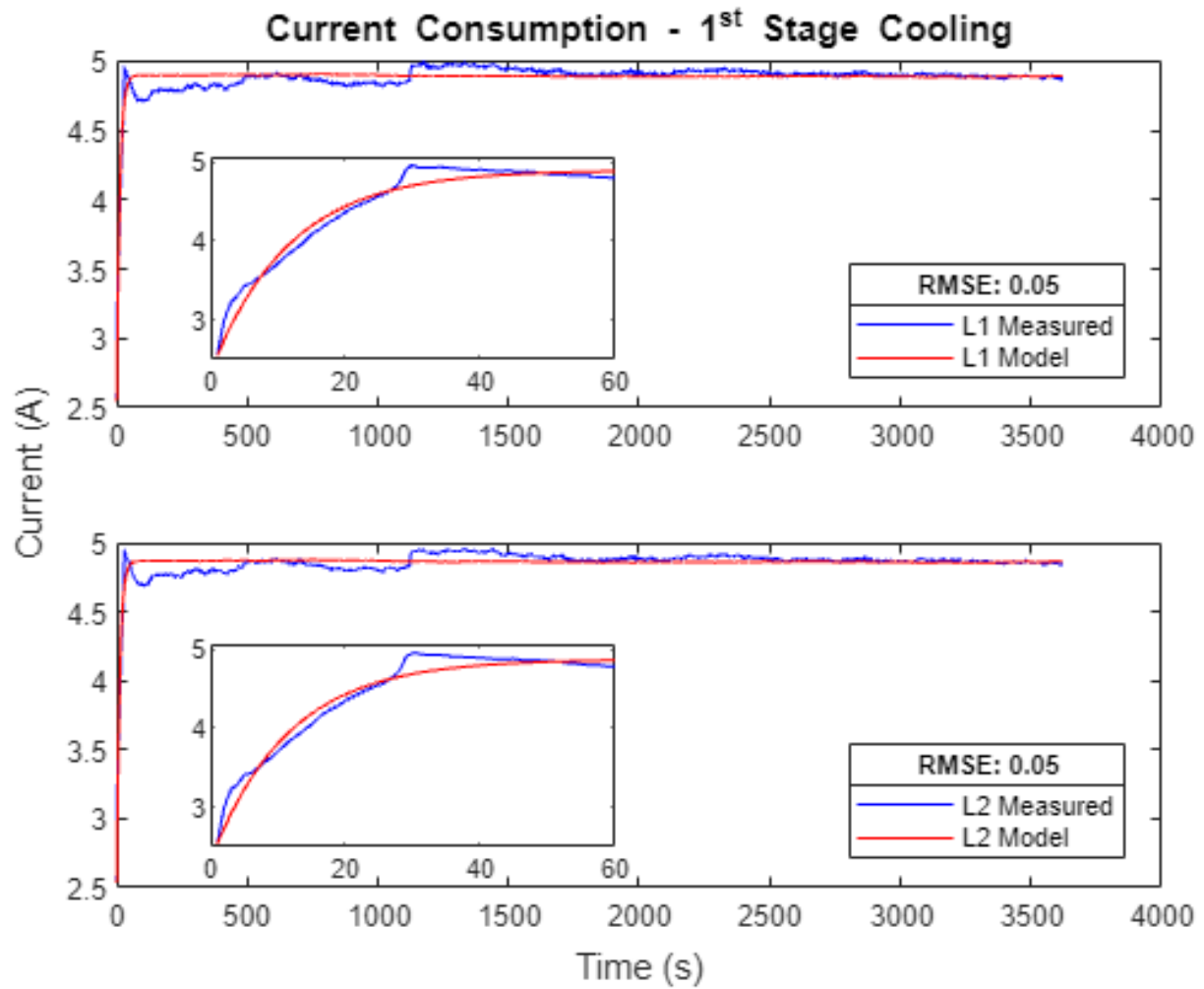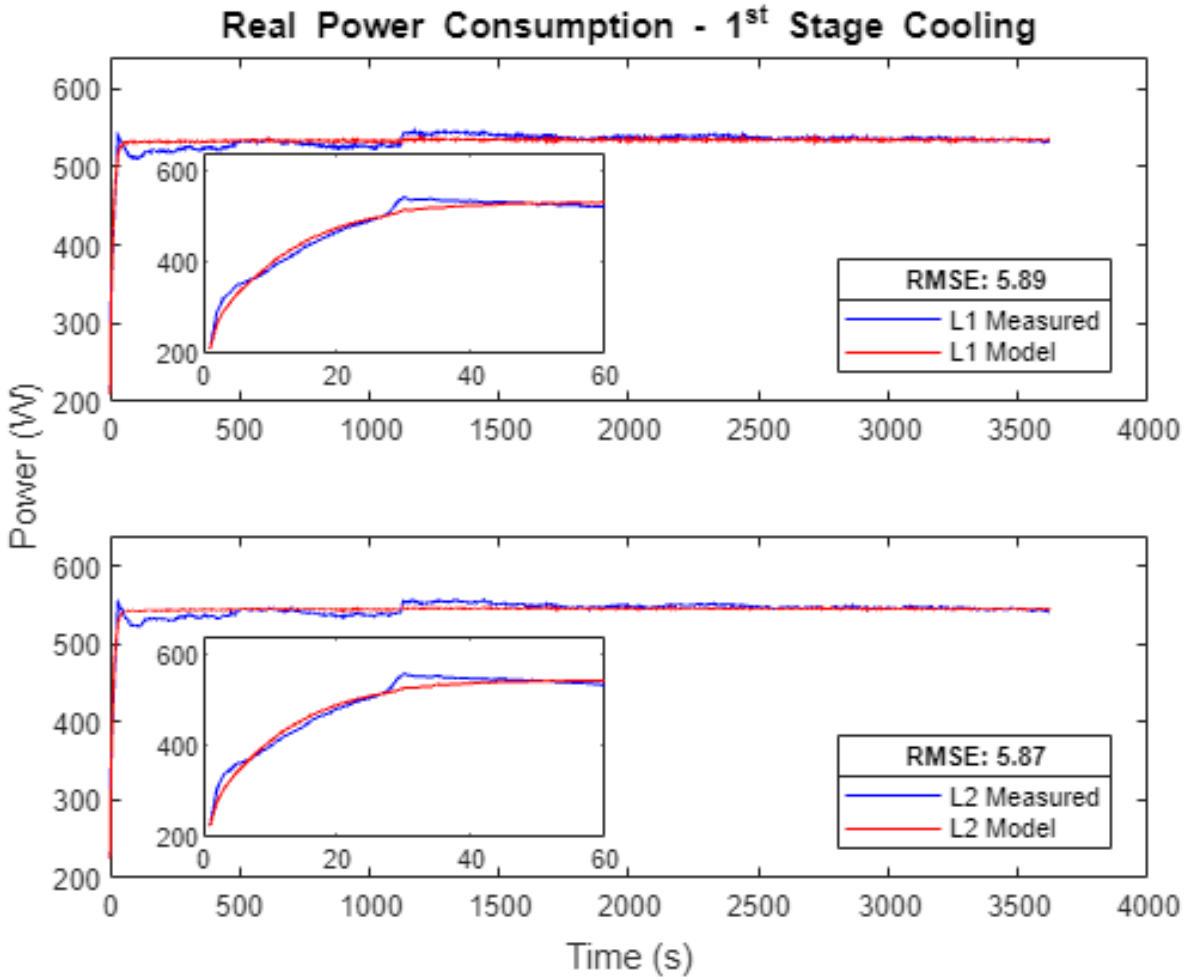

Fig. 17. Measured versus predicted current consumption of the heat pump on L1 and L2 phases during the 1st Stage of cooling
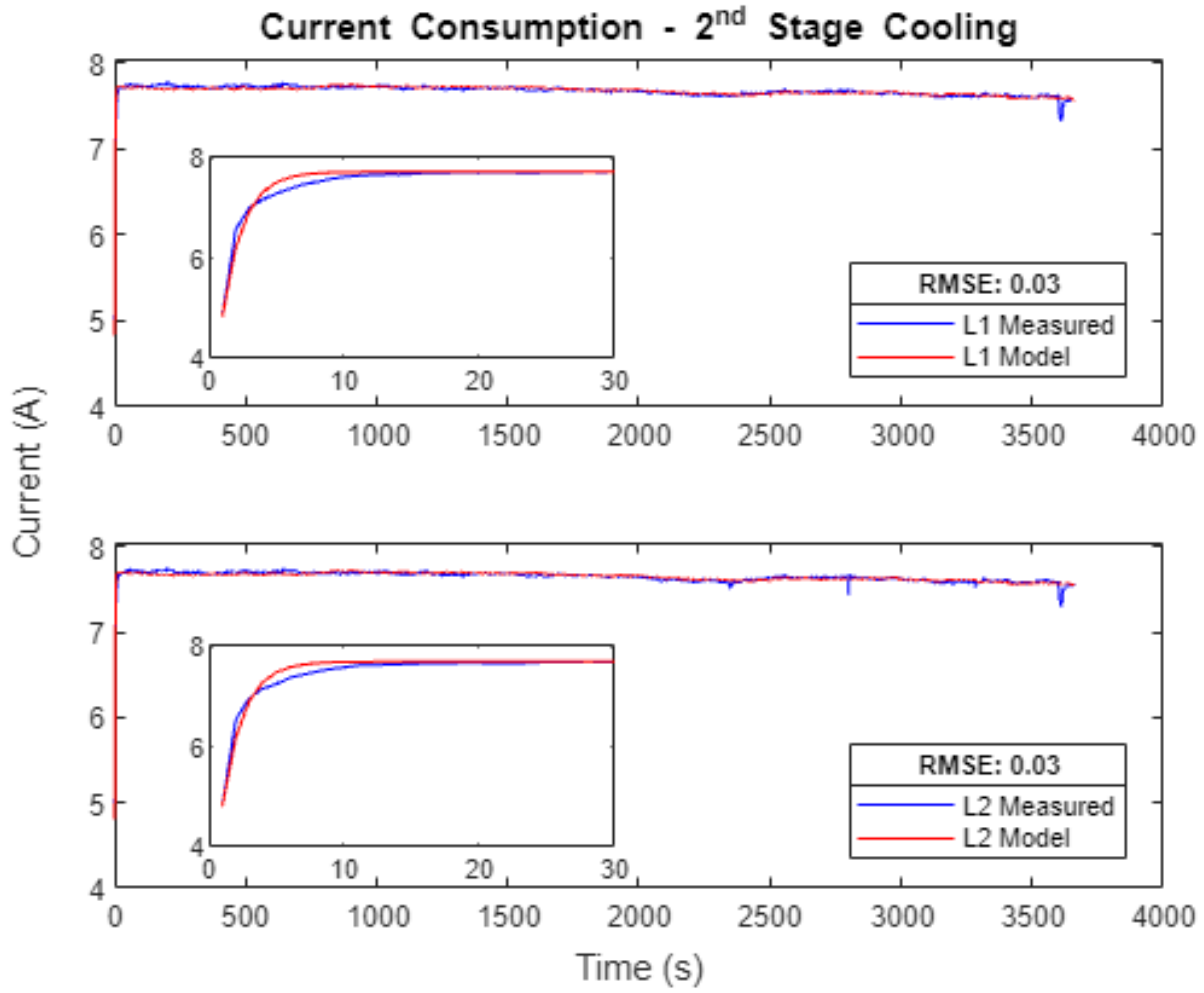
**Fig. 18.** Measured versus predicted current consumption of the heat pump on L1 and L2 phases during the 2nd Stage of cooling

Appendix B

The following figures depict a comparison between measured and predicted values of the real and reactive power consumption of the two-stage heat pump during the cooling season.

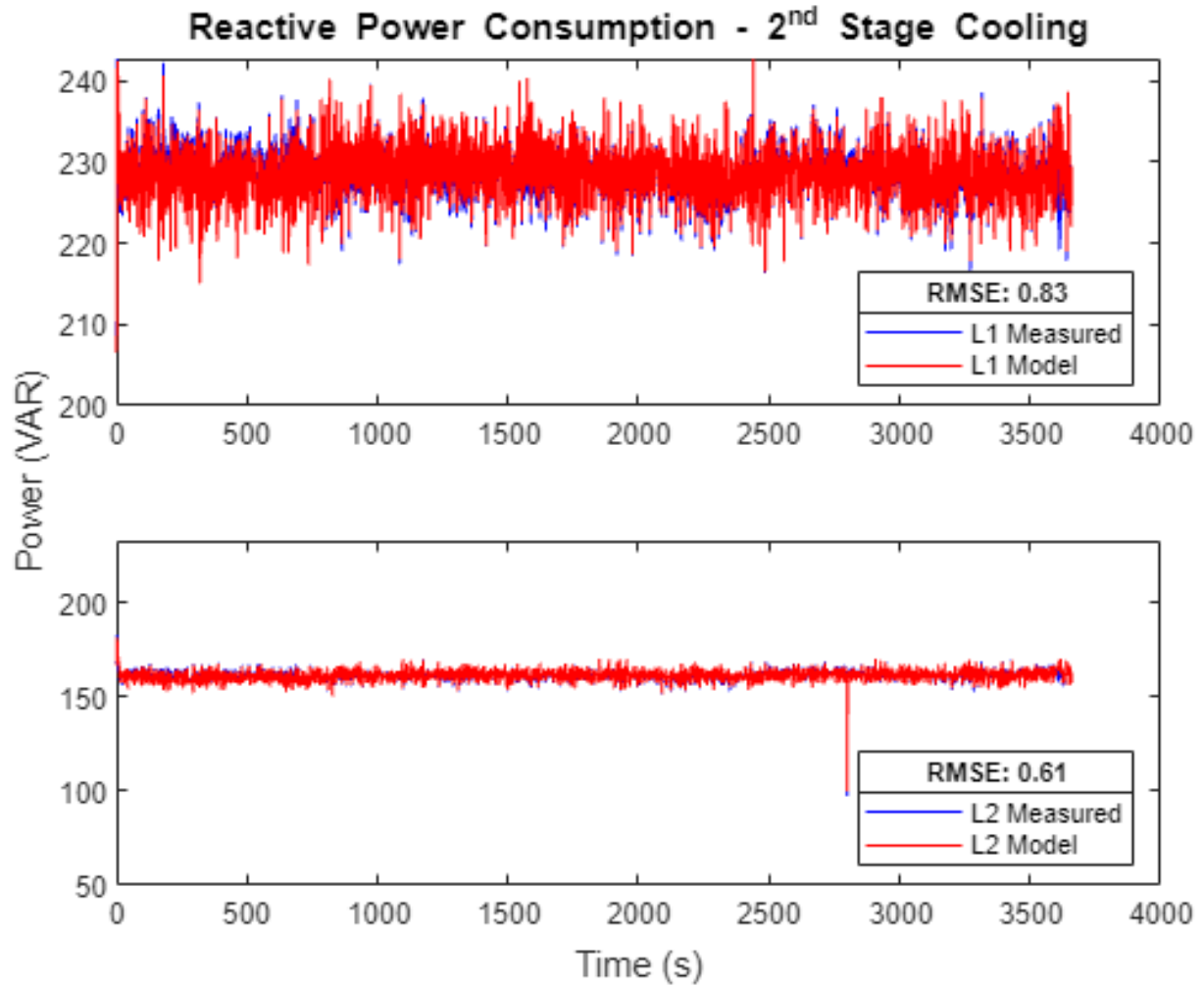**Fig. 19.** Measured versus predicted real power consumption of the heat pump on L1 and L2 phases during the 1st Stage of cooling
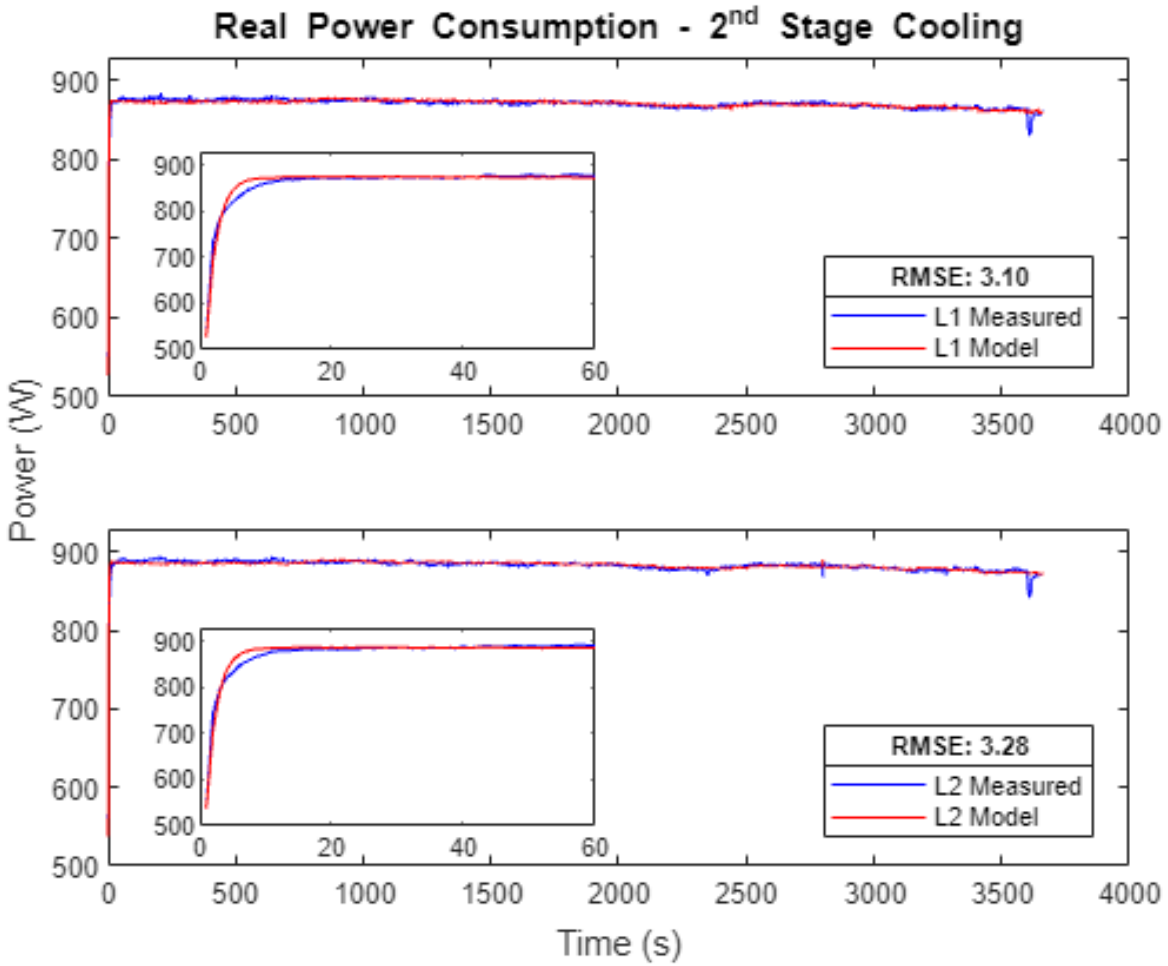
Fig. 20. Measured versus predicted real power consumption of the heat pump on L1 and L2 phases during the 2nd Stage of cooling
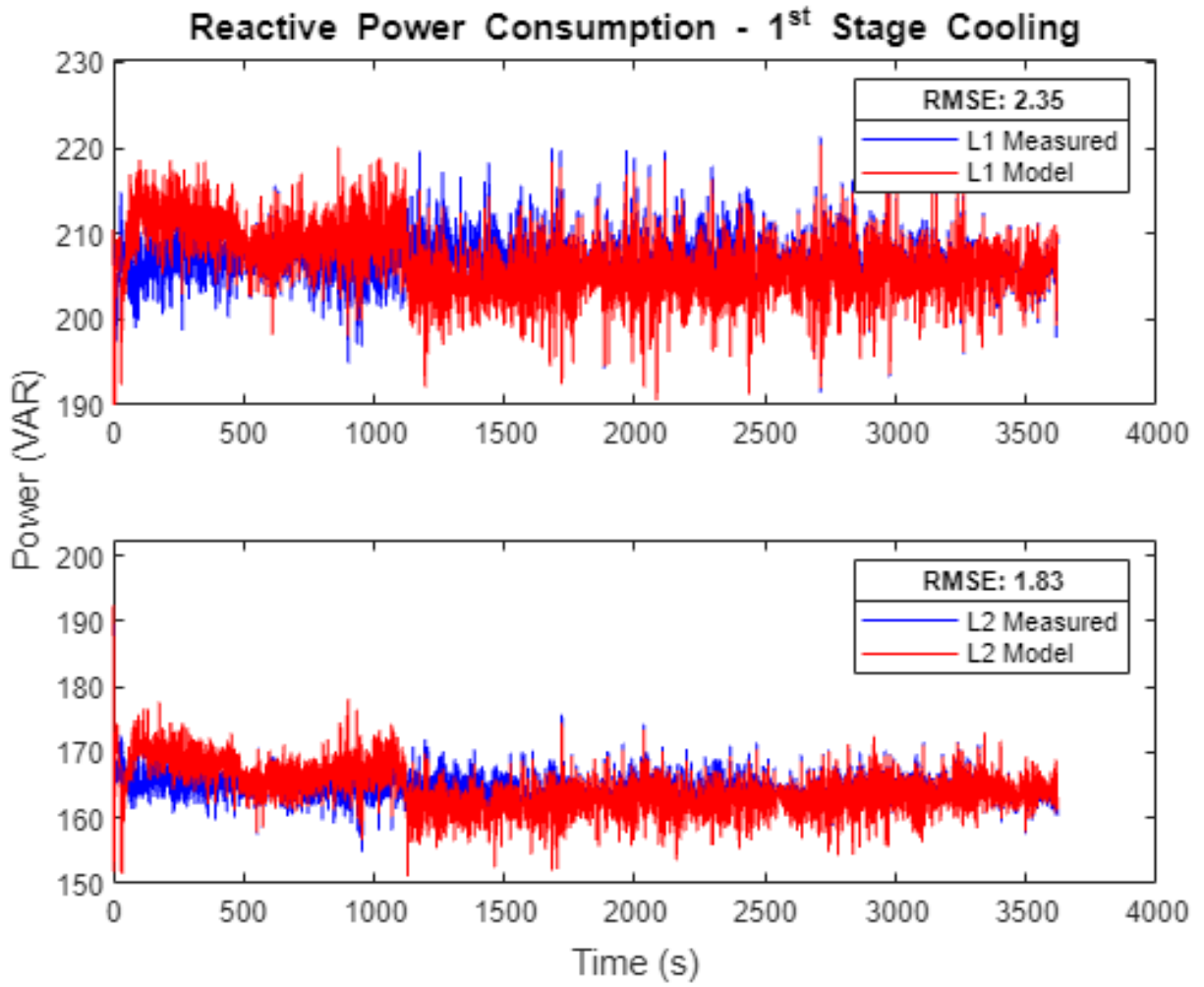
Fig. 21. Measured versus predicted reactive power consumption of the heat pump on L1 and L2 phases during the 1st Stage of cooling

Fig. 22. Measured versus predicted reactive power consumption of the heat pump on L1 and L2 phases during the 2nd Stage of cooling

References

[1]   NIST (2021) NIST Framework and Roadmap for Smart Grid Interoperability Standards, Release 4.0. *NIST Special Publication 1108r4* https://doi.org/https://doi.org/10.6028/NIST.SP.1108r4

[2]   Schwartz L, Leventis G, Zetterberg J (2020) Grid-Interactive Efficient Buildings: An Introduction for State and Local Governments FOR MORE INFORMATION Regarding Grid-interactive Efficient Buildings: An Introduction for State and Local Governments, please contact. (April). Available at www.seeaction.energy.gov

[3]   Lee ZE, Sun Q, Ma Z, Wang J, MacDonald JS, Max Zhang K (2020) Providing Grid Services With Heat Pumps: A Review. *ASME Journal of Engineering for Sustainable Buildings and Cities* 1(1):1–11. https://doi.org/10.1115/1.4045819

[4]   U.S. Department of Energy (2011) Load Participation in Ancillary Services. Available at https://www1.eere.energy.gov/analysis/pdfs/load_participation_in_ancillary_services_workshop_report.pdf

[5]   Holmberg D, Omar F (2018) Characterization of Residential Distributed Energy Resource Potential to Provide Ancillary Services. *NIST Special Publication 1900-601*:36. Available at https://doi.org/10.6028/NIST.SP.1900-601

[6]   Fuller JC, Vyakaranam BGNVSR, Kumar NP, Leistritz SM, Parker GB (2012) Modeling of GE Appliances in GridLAB-D: Peak Demand Reduction. (PNNL-21358):157. Available at http://www.pnnl.gov/main/publications/external/technical_reports/PNNL-21358.pdf

[7]   Fischer D, Madani H (2017) On heat pumps in smart grids: A review. *Renewable and Sustainable Energy Reviews* 70(November 2016):342–357. https://doi.org/10.1016/j.rser.2016.11.182

[8]   Arif A, Wang Z, Wang J, Mather B, Bashualdo H, Zhao D (2018) Load modeling - A review. *IEEE Transactions on Smart Grid* 9(6):5986–5999. https://doi.org/10.1109/TSG.2017.2700436

[9]   IEEE P2781 (2021) IEEE Draft Guide for Load Modeling and Simulations for Power Systems. Available at https://ieeexplore.ieee.org/document/9586464?denied=

[10]   Zhang M, Wu Q, Member S, Bo T, Rasmussen H, Yang X (2021) Heat pumps in Denmark: Current situation of providing frequency control ancillary services. *CSEE Journal of Power and Energy Systems*:1–10. https://doi.org/10.17775/cseejpes.2020.06070

[11]   Kim YJ, Norford LK, Kirtley JL (2015) Modeling and analysis of a variable speed heat pump for frequency regulation through direct load control. *IEEE Transactions on Power Systems* 30(1):397–408. https://doi.org/10.1109/TPWRS.2014.2319310

[12]   Georges E, Quoilin S, Mathieu S, Lemort V (2017) Aggregation of flexible domestic heat pumps for the provision of reserve in power systems. *30th International Conference on Efficiency, Cost, Optimization, Simulation and Environmental Impact of Energy Systems, ECOS 2017*.

[13]   Afram A, Janabi-Sharifi F (2014) Review of modeling methods for HVAC systems. *Applied Thermal Engineering* 67(1–2):507–519. https://doi.org/10.1016/j.applthermaleng.2014.03.055

[14]   Poudel B, Shiwakoti R, Amiri E, Rastgoufard P, Field TE, Ramamurthy J (2019) Aggregate model of single phase induction motors. *2019 IEEE International Electric*

Machines and Drives Conference, IEMDC 2019:1373–1378.
https://doi.org/10.1109/IEMDC.2019.8785388

[15] Cresswell C, Djokić S (2008) Representation of Directly Connected and Drive-controlled Induction Motors. Part 1: Single-phase Load Models. *Proc International Conference on Electrical Machines*. https://doi.org/10.1109/ICELMACH.2008.4800118

[16] Maitra A, Gaikwad A (2006) Measurement-Based Load Modeling. (Palo Alto, CA). Available at www.epri.com

[17] Schneider KP, Fuller JC, Chassin DP (2011) Multi-state load models for distribution system analysis. *IEEE Transactions on Power Systems* 26(4):2425–2433. https://doi.org/10.1109/TPWRS.2011.2132154

[18] Omar F, Bushby ST (2013) Simulating Occupancy in The NIST Net-Zero Energy Residential Test Facility. *NIST Technical Note 1817*. https://doi.org/https://doi.org/10.6028/NIST.TN.1817

[19] Davis M, Healy W, Boyd M, Ng L, Payne V, Skye H, Ullah T (2004) Monitoring Techniques for the Net-Zero Energy Residential Test Facility. *NIST Technical Note 1854*. Available at http://dx.doi.org/10.6028/NIST.TN.1854

[20] Omar F (2022) Experimental Design for Measuring the Voltage and Current Waveforms of Appliance Usage in the NIST Net-Zero Energy Residential Test Facility. *NIST Technical Note 2238*. https://doi.org/10.6028/NIST.TN.2238

[21] Frigo G, Derviskadic A, Pegoraro PA, Muscas C, Paolone M (2019) Harmonic phasor measurements in real-world PMU-based acquisitions. *I2MTC 2019 - 2019 IEEE International Instrumentation and Measurement Technology Conference, Proceedings* 2019-May. https://doi.org/10.1109/I2MTC.2019.8826988

[22] Omar F, Holmberg D (2021) Load Forecasting Tool for NIST Transactive Energy Market. *NIST Technical Note 2181* (Gaithersburg, MD). https://doi.org/10.6028/NIST.TN.2181

[23] Payne WV (2013) NZERTF's Heat Pump Capacity Outputs. (Private Communications, National Institute of Standards and Technology, MD). Available at https://www.nist.gov/people/vance-wm-payne

[24] IEEE Power & Energy Society (2010) IEEE Std. 1459-2010, Definitions for the measurement of electric power quantities under sinusoidal non-sinusoidal, balanced or unbalanced conditions. *IEEE* https://doi.org/10.1109/IEEESTD.2010.5439063